Bioprocess Biosyst Eng (2007) 30:397–418
DOI 10.1007/s00449-007-0136-x

ORIGINAL PAPER

# Metabolic flux analysis for optimizing the specific growth rate of recombinant *Aspergillus niger*

**R. Gheshlaghi · J. M. Scharer · M. Moo-Young · P. L. Douglas**

Received: 4 April 2007 / Accepted: 31 May 2007 / Published online: 16 July 2007
© Springer-Verlag 2007

**Abstract** A comprehensive metabolic network comprising three intracellular compartments (cytoplasm, mitochondrion and peroxisome) was developed for *Aspergillus niger*. The metabolic flux network includes carbohydrate and amino acid metabolism in both anabolic and catabolic reactions. Linear programming was used for the optimization of the specific growth rates in combination with 37 measured input and output fluxes of the key metabolites to evaluate corresponding intracellular flux distributions throughout the batch fermentations. Logarithmic sensitivity analysis revealed that the addition of proline, alanine and glutamate benefited growth in defined media. The experimental observations and flux analysis showed that tyrosine was a potential candidate for biomass production improvement. Model predictions was verified by conducting batch and fed-batch fermentations and it was found that the addition of the four amino acids according to the predetermined schedule resulted in a 44 and 41% improvements in biomass and recombinant protein productions, respectively.

R. Gheshlaghi (✉) · J. M. Scharer · M. Moo-Young · P. L. Douglas
Department of Chemical Engineering,
University of waterloo, 200 University Avenue West,
Waterloo, ON, Canada N2L 3G1
e-mail: rgheshla@engmail.uwaterloo.ca

J. M. Scharer
e-mail: jscharer@engmail.uwaterloo.ca

M. Moo-Young
e-mail: mooyoung@uwaterloo.ca

P. L. Douglas
e-mail: pdouglas@uwaterloo.ca

**Keywords** *Aspergillus niger* · Hen egg white lysozyme · Metabolic flux analysis · Logarithmic sensitivity · Metabolic pathways

## Introduction

Filamentous fungi have been employed for producing economically important products such as antibiotics (e.g., penicillin and cyclosporin), organic acids (citric acid, fumaric acid), vitamins (biotin, thiamine), and commercially enzymes (glucoamylase, lipase). The natural ability of filamentous fungi to synthesize, glycosylate, and secrete high levels of protein products has made them potentially attractive hosts for heterologous protein production. For instance, the *Aspergillus* species have proven to be potentially useful for the expression of eukaryotic gene products such as hen egg white lysozyme HEWL [1], tissue plasminogen activator t-PA [2], and lactoferrin [3].

The overproduction of the desired product is the primary aim in any biotechnology-based industrial process. In this regard, several methods have been applied to increase the level of the desired products comprising bioprocess optimization [4], strain development [5], medium optimization [6, 7], and mathematical modeling [8]. Nowadays, it is possible to direct modifications in microorganisms by using recombinant DNA technique which enables blocking a byproduct pathway by deletion or increase the enzyme levels for the overproduction of the desired product. The problem is, however, to specify the locations and the level of enzyme modifications in the metabolic network, otherwise the implied efforts by genetic engineering techniques may not be rewarded with an equivalent improvement in strain enhancement. This shortcoming may be overcome by using a quantitative approach which is able to simulate the

behavior of the microorganism before applying any strain modification.

The analysis of metabolic fluxes can provide important information such as maximal product yields on a substrate, recognize bottlenecks in the overproduction of the desired product, and identify the energetic parameters [9–12]. The metabolic flux analysis is based on network stoichiometry and conservation of mass and does not require information regarding enzyme kinetics. Often, this may be formulated as a set of linear ordinary differential equations. The stoichiometric approach focuses on the topology of the system and evaluates the rate by which a metabolite converts into other metabolites. The great advantage of the stoichiometric approach is that it forms a set of linear algebraic equations at steady state, which enables linear optimization.

In this work an optimization approach was utilized to obtain the intracellular metabolic flux distribution for *A. niger* producing the recombinant protein, hen egg white lysozyme (HEWL). In our previous study the production of recombinant proteins in aspergilli has been shown to be strictly growth associated. Therefore, it is convenient to optimize the growth rate in order to optimize recombinant protein productivity. The specific recombinant protein yield, of course, is dependent on cellular metabolism. Using on-line databases [13, 14], published results [15–28], and our experimental results (i.e., flux measurements) the main objective was to develop an elaborated stoichiometric-based flux model to simulate the behavior of the microorganism, to determine the maximum theoretical specific growth rate and to predict the effect of any change in some fluxes on the behavior of the cells for subsequent perturbation studies. This *Aspergillus* strain has an absolute requirement for amino acids in the medium. One of the objectives in this work was to replace a complex nitrogen source (peptone) that was used in our previous studies [6] with a known mixture of amino acids. This enabled one to monitor the concentration of individual amino acids throughout the course of fermentation and use this information as the input for the model.

## Materials and methods

### Microorganism, inoculum preparation

A recombinant *Aspergillus niger* strain HEWL WT-13–16 was kindly provided by Dr Mackenzie (Institute of Food Research, Norwich Research Park, UK). A spore stock suspension was prepared [6] giving a stock conidia concentration of approximately $5 \times 10^7$ spores/mL. Approximately 1-mL aliquots of the spore suspension were dispensed into 1.5 mL Eppendorf tubes, and stored at –35 °C until required for inoculum preparation.

### Medium composition

Unless specified otherwise, the chemically defined medium contained (per liter): glucose 20 g, ammonium sulfate 3.1 g, amino acids mixture 3.2 g, and salt solution [29] 20 mL. The amino acid mixture in this study was based on the amino acid content of 0.5% (w/v) peptone (Becto$^{TM}$). The amino acid composition of the peptone was provided by manufacturer (Becton, Dickinson and Company). Unexpectedly, the glycine content of peptone was 16%, much higher than any of the other amino acid concentrations. The corresponding glycine concentration in the medium was 0.792 g/L. Two experiments with 0.792 and 0.396 g/L glycine were performed (not shown) while the other amino acids were supplied according to the peptone composition. No significant differences in lysozyme and biomass concentrations were observed. Therefore, for further experiments the concentration of glycine was maintained at 0.4 g/L. Accordingly, the composition of the amino acid mixture in the medium was (%w): Ala 14.3, Arg 8.9, Asp 7.7, Glu 12.5, Gly 12.5, His 1.2, Ileu 3.2, Leu 5.8, Lys 5.1, Met 1.3, Phe 4.3, Pro 13.5, Ser 2.3, Thr 1.7, Tyr 1.4, Val 4.3. Glucose and the inorganic salt solution were autoclaved separately for 20 min at 121 °C, and were added to filter-sterilized amino acids mixture to give the final medium.

### Fermentation

The preparation of inoculum for the bioreactor was carried out in 250 mL Erlenmeyer flasks containing 45 mL of medium along with 5 mL of sterilized sodium citrate/citric acid (0.97 M, pH 6.5) as buffer. The citrate buffer was autoclaved separately and then added to the medium to prevented the formation of a precipitate [30].The initial medium pH was adjusted to 6.00 with NaOH. This initial pH was found to have a beneficial effect on growth of this strain of *A. niger* [31, 32]. The flasks were inoculated with 40 μL spore stock suspension to give a final concentration of approximately $4 \times 10^4$ spores/mL in each flask. These cultures were grown at 27 °C and 200 rpm for 48 h on an Innova 4330 refrigerated incubator shaker (New Brunswick Scientific Co, USA).

Batch fermentation experiments were performed in either a 2-L Bioflo fermenter (New Brunswick Scientific Co, NJ) with a working volume of 1.5 L, or a 7-L Applikon bioreactor (Applicon Dependable Instruments, Holland) with the working volume of 4.5 L using the medium described above. The bioreactor cultures were inoculated with a mycelial inoculum size of 5 or 3.3% of working volume for 2 or 7-L bioreactors, respectively. The culture temperature was kept at 27 ± 0.5 °C. Air was supplied at a rate of 1 vvm and was sterilized through a hydrophobic 0.2 μm (Millipore) membrane filter. The broth was mixed

using three six-bladed Rushton turbine impellers rotating at 200–400 rpm. The dissolved oxygen was monitored and kept at above 20% of the saturation value using variable agitation schemes. The initial pH of the broth was adjusted to 6.0 and the fermentations were operated without any pH control until it decreased to a set point of 4.0. After reaching this set point, the pH was maintained at 4.0 ± 0.1 by adding either 2 M sodium hydroxide or 2 M sulfuric acid by an automatic pH-control system using a sterilizable probe mounted in the reactor. To prevent excessive foaming, antifoam (Sigma 204) was added, as needed.

### Analytical procedures

The samples were analyzed for concentrations of cells, glucose, 10 organic acids, 20 amino acids, ammonia, phosphate, and sulfate throughout the fermentation. Each analysis was carried out in triplicate. There was no significant difference between the triplicate analyses at the confidence level of 90%, so the average of each set of measurements was reported and employed in this study. To assess the accuracy and reproducibility of the HPLC analysis for amino acids, the concentration of each amino acid detected at the beginning of the fermentation was compared with the concentration supplied. Maximum errors were 18 and 15% for glycine and serine, respectively. The associated error was determined to be 12% for the initial concentration of ammonia.

### Biomass concentration

Biomass concentration was determined by dryweight measurements. The sampling device was modified to provide representative samples of the culture. 3 × 5 mL samples were taken at specific time intervals and filtered on predried, preweighed filters (4.25 cm GF/C filter, 1.2μm, Whantman No. 42) under vacuum. Filter cakes were washed with distilled water twice and dried at 80 °C for at least 24 h to constant weight. The filtrate was stored at –35 °C for further analysis.

### Off-gas analysis

Carbon dioxide and oxygen concentrations were monitored online at the inlet and outlet of the fermenter with a solid-sate infrared $CO_2$ sensor and an electrochemical oxygen sensor, respectively (Model 902, Quantek Instruments, USA).

### Analysis of filtrate samples

Glucose content was analyzed enzymatically by a glucose kit (Megazyme Glucose Test Kit). Ammonia was measured using a pH/ISE meter model 710A with an ammonia gas-sensing Ion-selective electrode (Beckman). Amino acids and low molecular weight organic acids were measured with a reversed phase HPLC system (Varian analytical Instruments, USA). The column was a 150 × 4.6 mm Inertsil C8-3 with the particle size of 5 μm. The organic acid content of the fermentation samples were quantified using the method described by Gawthray [33]. All the samples and standards were acidified to pH 2.7 with *ortho*-phosphoric acid. He proposed a mobile phase with the composition of 93% 25 mM $KH_2PO_4$ and 7% methanol at the total flow rate of 1 mL/min. However, it was found that using a mobile phase of 99.5% 25 mM $NH_4H_2PO_4$ and 0.5% methanol with the total flow rate of 0.7 mL/min gave better separation for most of the organic acids under study using the HPLC system outlined in this section. Accordingly, the concentrations of oxaloacetate, acetate, α-ketoglutarate, citrate, fumarate, malate, pyruvate, oxalate, gluconate, and succinate were determined at 210 nm and temperature of 27 °C. The co-elution between gluconate and oxalate was not prevented by the proposed system, so the first peak in the samples was the sum of absorbance of gluconate and oxalate peaks. Therefore, concentration of gluconic acid in each fermentation sample was determined enzymatically by a specific kit for gluconic acid (Megazyme gluconic acid kit). The absorbance of each sample solution was monitored over a period of 30 min. The conversion of gluconic acid was found to be completed in 15 min after the addition of the last reagent. The concentration of gluconic acid and the area of the first peak in the chromatogram of each sample (as the indicator of both acids) along with the calibration curve of both acids were used for calculating the oxalic acid content of the corresponding sample. The 20 L-amino acids were analyzed using the precolumn derivatization technique with PITC [34] at 50 °C with some modifications. Phosphate and sulfate were measured using an Ion Chromatography system (Dionex, DX 500 Chromatographic system, USA).

## Model construction

The detailed information pertaining to the model construction is described elsewhere [35]. A brief description of the stoichiometric model is given below. The model for growth and product formation of *A. niger* has been developed using published information for this microorganism. Moreover, in case there was not specific information for *A. niger*, corresponding data of closely related filamentous fungi (e.g., *A. nidulans*) were included, and as a last resort, data obtained for yeasts (e.g. *Saccharomyces cerevisiae*) were utilized when data were completely lacking or inadequate. This reaction network includes glycolysis and pentose phosphate (PP) pathways, tricarboxylic acid cycle

(TCA), anaplerotic reactions, ammonia and sulfate assimilation, electron transport reactions, biosynthesis and degradation of amino acids, and the biosynthesis of nucleotides and macromolecular components of biomass. The anabolic reactions for *A. niger* for protein, lipid, RNA, DNA, and biomass synthesis were taken from the reported information for *A. oryzae* at the specific growth rate of 0.1 $h^{-1}$ [15]. In this study, a single reaction (*R11.5*) based on a fixed biomass composition was employed for the formation of biomass throughout the fermentation. Since, several studies failed to produce evidence for the Entener–Doudoroff (ED) pathway in fungi [36, 37] this pathway was not included in the model. The proposed metabolic model for *A. niger* consists of three compartments. The cytosolic compartment contains the reactions comprising glycolysis, gluconeogenesis, the PP pathway, and the majority of anabolic pathways. The mitochondrial compartment includes the TCA cycle, the biosynthesis pathways of the amino acids isoleucine, valine, arginine, part of the biosynthesis of leucine and lysine, and oxidative phosphorylation; and the peroxisomes fraction, which contains the glyoxylate shunt. For *A. niger* some researchers claim only mitochondrial localization of pyruvate carboxylase [38], whereas others find the enzyme in both the cytosolic and mitochondrial fractions [39]. Considering these findings, pyruvate carboxylase was assumed to be present in both the cytosol and mitochondrion. The operational P/O ratios for the oxidation processes in *A. niger* were reported to be 1.5–1.8 for $FADH_2$, 2.3–2.7 for $NADH_m$, and 1.4–1.8 for $NADH_c$ [40]. The operational P/O ratios for the oxidation of $NADH_m$, $FADH_2$, and $NADH_c$ in our simulations were 2.64, 1.64, and 1.64, respectively.

A schematic outline of the major metabolic pathways is depicted in Fig. 1. The complete set of reactions of the metabolic network with corresponding reaction numbers is given in "Appendix B".

## Mathematical formulation

### Metabolite balancing

Assuming pseudo-steady state in the metabolite concentrations and negligible dilution effects for growth [41], the general equation for cellular metabolism in matrix notation is given as follows:

$$S \cdot V = 0 \tag{1}$$

The matrix $S$ contains the stoichiometric coefficients and the vector $V$ represents the fluxes in the metabolic network. If a system boundary around the cell is considered, this boundary is closed to the passage of certain metabolites while others are allowed to enter or exit the system based on external sources or sinks. Should an external source or sink of a metabolite exist, the introduction of an exchange flux is necessary to allow a metabolite to enter or exit the system boundary. These fluxes have been referred to as pseudo-reactions [42] and can be thought of as representing the inputs and outputs to the system. It is possible to reduce the degree of freedom of the set of algebraic equation by measuring some of these exchange fluxes. Then, the vector of fluxes can be partitioned into unknown internal fluxes $V_u^I$, unknown exchange fluxes $V_u^E$, and known (measured) exchange fluxes $V_k^E$. In the same manner, the matrix $S$ can be partitioned into $S_u^I$, $S_k^E$, and $S_k^E$. Upon substitution into Eq. (1) and rearrangement one obtains the following:

$$S_u^I V_u^I + S_u^E V_u^E = b \tag{2}$$

Where $S_u^I$ is an $m \times n_u^I$ matrix, $S_u^E$ is an $m \times n_u^E$ matrix, $m$ is the number of metabolites, $n_u^I$ and $n_u^E$ are the number of unknown intracellular and exchange fluxes, respectively. For the sake of simplicity the negative product of $S_k^E$ and $V_k^E$ is replaced by vector $b$, which is an $m \times 1$ vector. The elements of vector $b$ (i.e., $b_i$) were evaluated from the slope taken between two consecutive concentration data points. In our model, these elements were defined as positive outward, thus the numerical value of each element of $b$ was negative, when a metabolite was entering the system and positive when it was exiting the system. Equation (2) shows the fundamental relation in metabolic balancing.

### Linear programming

As the number of unknown fluxes $n_u$ is typically greater than the rank($S_u$) the system is underdetermined and the degree of underdeterminacy will increase as the network becomes more complex due to the larger number of branch points in the network.

Consequently, the number of feasible flux distributions allowed by the Eq. (2) is infinite. The metabolic flux distribution may be estimated by formulating a suitable objective function and using linear programming [43]. The linear programming can be formulated as:

$$\begin{aligned} \text{Max} \quad & Z = \sum \varpi_j v_j \\ \text{subject to:} \quad & S_u^I V_u^I + S_u^E V_u^E = b \\ & (1-\varepsilon_i) b_i \le b_i \le (1+\varepsilon_i) b_i \\ & 0 \le v_{u,j}^I \le \gamma_j \\ & v_{u,i,\min}^E \le v_{u,i}^E \le v_{u,i,\max}^E \end{aligned} \tag{3}$$

where, weighting element $\varpi_j$ specifies the importance of the corresponding individual flux of $v_j$ in the objective function of $Z$. In the present work, the unknown fluxes that are the model variables were expressed in units of (mmol/

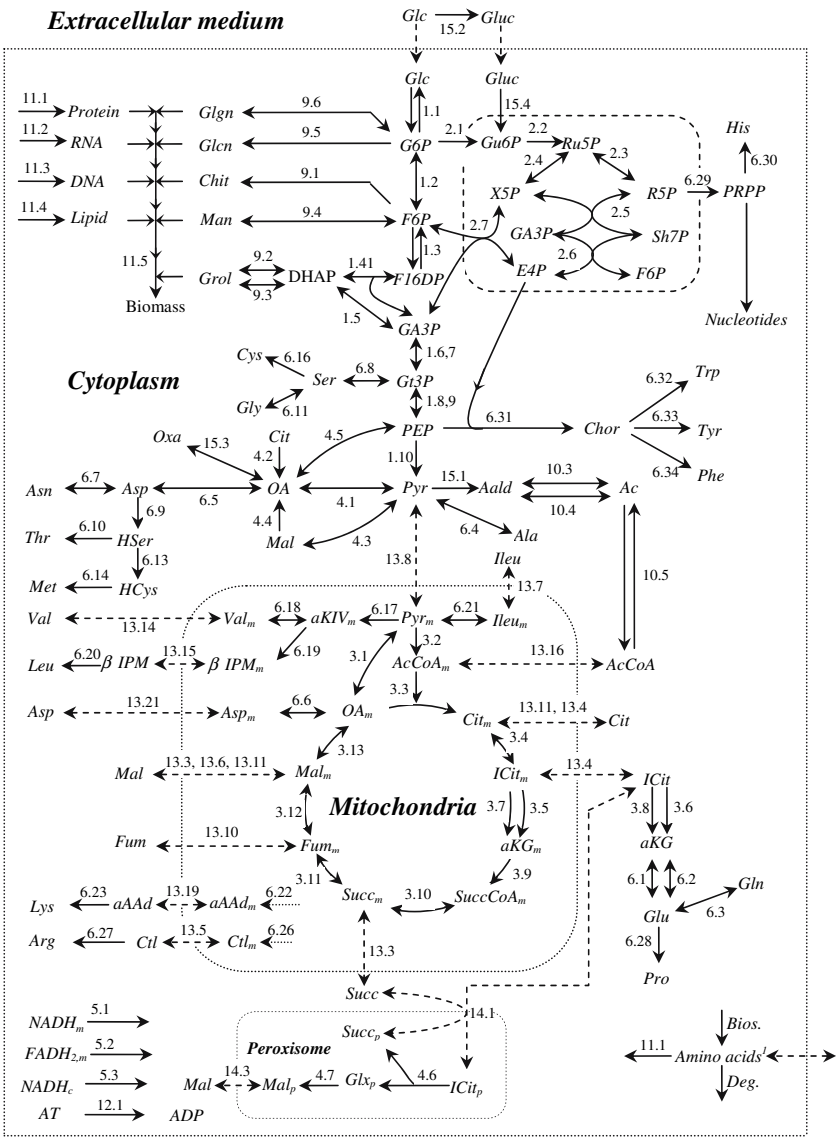


**Fig. 1** The general overview of the proposed metabolic pathways for *A. niger* (refer to the "Appendix A" for list of symbols). Three compartments cytoplasm, mitochondria, and peroxisomes are distinguished. The *solid* and *dashed arrows* with the reaction numbers next to them represent metabolic reactions and transport processes, respectively. The abbreviations and corresponding reactions are given in the Appendix. For the amino acids four different fluxes have been included in the model: biosynthesis, degradation, transport between cytoplasm and abiotic phase, and for protein biosynthesis; however, for simplicity only the first set is shown in the map

$g_{DW}$ h) and the normalized biomass flux represented the specific growth rate, $\mu$(1/h). In this work, the objective function was the specific growth rate. The first set of constraints is simply the steady state flux balances. The second set of constraints introduces the vector of parameters $\varepsilon_i$, which accounts for any possible error involved with the measured fluxes. The introduction of error limits has been proposed by Lee and Papoutsakis [44], but to our knowledge has not been employed previously. In this study, the measured flux limits were based on error observed during the triplicate experimental analysis.

The solution vector, $v^{I}_{u,j}$ and $v^{E}_{u,i}$, of the linear programming problem will be always non-negative due to the characteristics of the Simplex algorithm. Consequently, reversible reactions must be formulated as two separate reactions, one in forward direction, and the other in the reverse direction. This property allows to the incorporation of coarse thermodynamic information by distinguishing between reversible and nearly irreversible reactions in the stoichiometric matrix [45]. The third set of constraints simply states this property for unknown internal fluxes. Further, the upper limit of this set (i.e.,$\gamma_j$) could be representative of a maximum allowable flux through a given reaction, resulting from a limited amount of an enzyme presented [44]. The last set of constraints implies upper and lower bounds on each exchange flux that represents the corresponding metabolite's potential to enter or exit the system. There can only be one exchange flux per metabolite. The value of these exchange fluxes was considered to be zero if the system was closed to the passage of the metabolite (e.g., mitochondrial and peroxisomal metabolites), positive if the metabolite was either exiting or being produced by the system, and negative if the metabolite was entering or being consumed by the system. However, to

comply with the Simplex algorithm and make the mathematical procedure more straightforward all exchange fluxes need to be considered non-negative. To overcome this drawback for entering metabolites, one can define all the exchange fluxes as positive and at the same time consider the corresponding member of the entering metabolites in matrix $S_u^E$ positive one instead of negative one. This convention for reversible reactions and exchange fluxes is used merely for mathematical purposes and does not influence the biological interpretation of metabolic function in any way. Linear programming calculations were performed in a GAMS environment [46].

### Sensitivity analysis

Since experimental data are subject to analytical errors, the assigned value is only an estimate [47]. The sensitivity of the objective function $Z$ with respect to the change of the $i$th measured exchange flux was determined using the shadow price [48] of the linear programming which is defined as follows:

$$\lambda_i = \frac{\partial Z}{\partial b_i} \tag{4}$$

The shadow price values were computed from the mathematical duality of the primary linear optimization problem. The shadow price needs to be considered for improving the optimal solution with respect to the sign of the corresponding exchange flux. For instance, one can ameliorate the optimal solution by increasing substrate uptake rates and/or by decreasing by-product excretion rates of the metabolite with negative shadow prices.

Moreover, since the absolute value of the exchange fluxes vary substantially, the relative or logarithmic sensitivity was used for comparison purposes. The sensitivity value quantifies the relative change in a calculated variable that is evoked by a relative change in a system parameter [49, 50]. The logarithmic sensitivity of the objective function in response to the change in the $i$th measured flux can be expressed as follows:

$$\Lambda(Z, b_i) = \frac{\partial Z/Z}{\partial b_i/b_i} = \frac{\partial \operatorname{Ln} Z}{\partial \operatorname{Ln} b_i} = \frac{b_i}{Z}\lambda_i \tag{5}$$

As shown in Eq. (5), only shadow price values, the measured exchange fluxes, and the optimal value of the objective function are needed to compute the logarithmic sensitivities.

## Experimental results

To ensure that all metabolites and cell components are accounted for, detailed overall nitrogen and carbon mass balances were performed using the measured data (not shown). Mass balance calculations included sets of 37 measurements taken at approximately 6–12-h intervals for 120 h of total fermentation time. Both the carbon and nitrogen balances could be closed with a maximum error of 11%.

Two fermentations were performed under identical conditions and the averages of the two set of observations were used. Profiles of the measured extracellular compounds in *A. niger* batch culture are illustrated in Figs. 2, 3, 4. The profiles were found to be reproducible, since fermentation repeats produced almost identical results. For example, the maximum relative error of 14% at the 48th hour of the fermentations was observed between the biomass concentrations of the two fermentations. The average relative error was determined to be 9.8% throughout the course of the fermentations.

Figure 2 shows the concentration profiles of glucose, biomass, lysozyme, gluconate, and oxalate throughout the course of the fermentation. Glucose is consumed initially and its concentration decreased to zero after 30 h of the fermentation. Much of the glucose was converted to gluconate reaching a maximum concentration of 16.2 g/L after 30 h. Considering the glucose supply, (i.e., inoculum and fermenter) the concentration of gluconate accounted for approximately 74% of the converted glucose. The oxalate concentration increased monotonically throughout the fermentation reaching a maximum value of 5.6 g/L after 120 h.

The concentration profiles of the minor organic acids are depicted in Fig. 3. Succinate and acetate accumulated during initial 24–30 h of the process to the maximum levels of 0.39 and 0.17 g/L, respectively. The concentration of citrate at the beginning of the fermentation was measured to be 1.3 g/L, which was added as citrate buffer

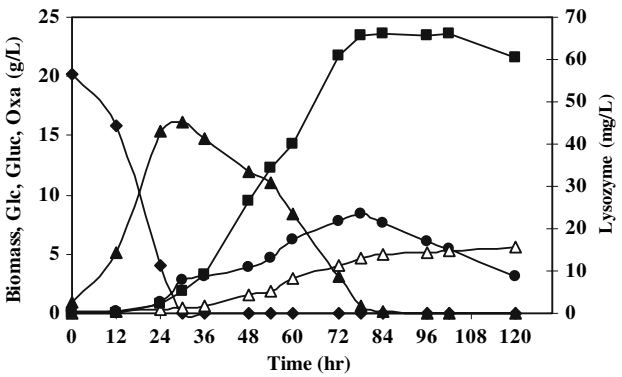


**Fig. 2** Glucose, biomass dry weight, gluconate, oxalate, and lysozyme concentration profiles during the fermentation. $T$ = 27 °C, $N$ = 400 rpm, and aeration 1 vvm. Glucose (*filled diamond*), biomass dry weight (*filled circle*), gluconate (*filled triangle*), oxalate (*open triangle*), and lysozyme (*filled square*)

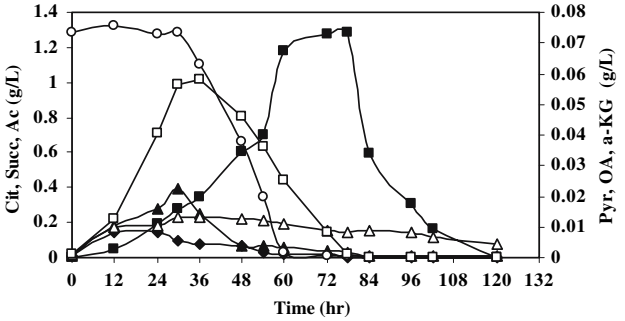


**Fig. 3** Organic acid concentration profiles during the fermentation. Citrate (*open circle*), acetate (*filled diamond*), succinate (*filled triangle*), a-ketoglutarate (*open triangle*), pyruvate (*filled square*), oxaloacetate (*open square*). $T$ = 27 °C, $N$ = 400 rpm, and aeration 1 vvm

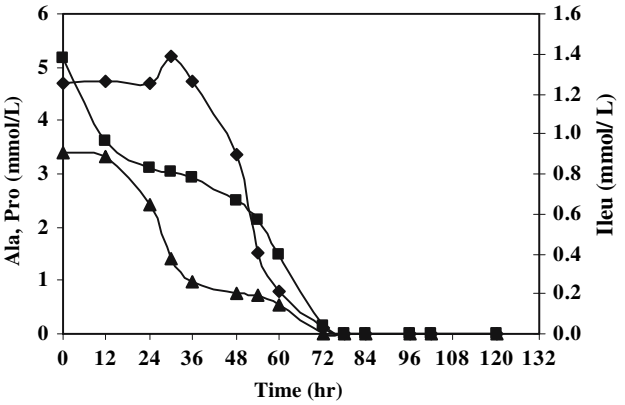


**Fig. 4** The typical amino acids concentration profiles during the fermentation. $T$ = 27 °C, $N$ = 400 rpm, and aeration 1 vvm. Alanine (*filled diamond*), proline (*filled triangle*), and isoleucine (*filled square*)

initially. The citrate concentration was nearly constant during the early stage of the fermentation and then dropped to zero by the middle of the process. Pyruvate accumulated during the growth phase and then its concentration declined to zero during the death phase, however, its maximum concentration of 0.075 g/L was very low. Oxaloacetate concentration increased to the maximum level of 0.056 g/L at the 36th hour of the fermentation and then fell to zero. Malate and fumarate were not detected in the culture medium during the entire time course of the fermentation. There is no evidence for any external accumulation of fumarate by *A. niger* [20].

Amino acid consumption was variable. The concentration profiles could be categorized into three distinct groups. For sake of clarity only the profile of one amino acid in each group is given in Fig. 4. The first group consisted of alanine, arginine, aspartate, cysteine, glutamate, glycine, and lysine. The concentration of these amino acids remained relatively constant during the first 24 h of fermentation while glucose was consumed. Then the profiles passed through a maximum and dropped sharply until the concentrations became zero, with the exception of glycine which remained nearly constant after 72 h of the fermentation at 0.45 mmol/L. The commencement of amino acid consumption coincided with a sharp decline of the specific growth rate.

The concentration profile of the second group (isoleucine, leucine, phenylalanine, threonine, and tyrosine) decreased throughout the fermentation with particularly high rate during the first 12 h; then either decreased slowly or remained relatively constant, and finally fell to zero at a relatively high rate. Phenylalanine was the only member whose concentration did not drop to zero but remained constant after 60 h at a low level of approximately 0.04 g/L which was 4.4% of its initial concentration.

Proline, histidine, methionine, serine, and valine comprised the third group, which did not possess similar trends as the first two groups. For instance, valine and serine were not utilized until late in the fermentation. The utilization of proline, on the other hand, appeared to be biphasic.

Considering glucose, biomass, lysozyme, amino acids, organic acids, and other metabolite profiles the fermentation could be conveniently divided into five distinct phases.

Phase I ($0 < t < 12$ h), was the early stage of the fermentation, when the culture was in the lag phase and both biomass and lysozyme concentrations were very low. The glucose concentration, however, decreased by 22%. The concentration of gluconate at the end of this phase reached to 5.4 g/L. Based on these observations, gluconate production alone accounted for approximately 93% of glucose consumption. Amongst the amino acids, leucine, isoleucine, and phenylalanine had the highest specific uptake rates of 0.18, 0.14, and 0.13 mmol/$g_{DW}$ h, respectively. Although succinate, acetate, and oxalic acid were accumulated in the extracellular medium, the high specific excretion rate of gluconate (10.1 mmol/$g_{DW}$ h) was the main reason for the pH drop from 6 to 4.

In phase II ($12 < t < 24$ h), cell concentration commenced to increase, while the lysozyme concentration remained still low. The glucose consumption rate was high and the concentration decreased to 25% of the initial level while the biomass dry weight level reached nearly 1 g/L by the end of this period. The concentration of gluconate, the main organic acid component in the culture medium increased to 15.3 g/L. From these observations one could conclude that the activity of glucose oxidase enzyme was high during this phase of fermentation. The concentration of all amino acids decreased during this phase with proline having the highest specific uptake rate. The oxygen consumption rate was approximately threefold higher than during the first period.

During Phase III ($24 < t < 30$ h) glucose was consumed fast and its concentration dropped to essentially zero

(i.e., 0.01 g/L) while gluconate concentration reached a maximum level of 16.2 g/L by the end of this phase. Acetate was the only organic acid with decreasing concentration albeit at a relatively low rate. As the time approached to the end of this phase, succinate concentration increased to its maximum value of 0.4 g/L. The oxygen uptake rate was 1.5 times higher than that of the second phase. The specific carbon dioxide evolution rate peaked during this phase of the fermentation. The first group of the amino acids along with methionine, valine, and serine started to accumulate in the medium, whereas the concentration of the second group decreased. The specific growth rate reached its maximum value of 0.177 $h^{-1}$, consequently the cells produced the recombinant protein in higher levels than in previous phases.

At the end of Phase IV ($30 < t < 78$), the concentrations of biomass, lysozyme, and pyruvate reached to their maximal value. Gluconate was the main carbon source in the medium and its concentration decreased to 0.6 g/L by the end of this phase showing 96% reduction in the concentration in comparison to its maximum value. Oxalate concentration increased throughout this phase to the final level of 4.6 g/L. This time period is characterized by high amino acid metabolism. Most amino acids were consumed during this phase.

Phase V ($78 < t < 120$ h), is the last phase of the fermentation. Basically, it represents the death phase, when the biomass concentration decreased. With the notable exception of pyruvate, the concentrations of extracellular metabolites showed no significant changes. The pyruvate concentration continued to decrease to zero by the end of this phase. Product formation ceased as the culture entered this phase and the specific growth rate become negative. For these reasons, this phase was not analyzed further.

## Metabolic flux distribution

Using experimental data, the extracellular metabolite fluxes were calculated from the metabolite concentration profiles for each phase. In order to verify the result of each simulation, the oxygen uptake and the carbon dioxide evolution rates were allowed to be determined by the optimization program. Employing the specific growth rate as the objective of the optimization program, the predicted specific growth rate, the specific oxygen uptake, and carbon dioxide evolution rates along with the corresponding experimental measurements are presented in Table 1.

Logarithmic sensitivities of the objective function with respect to amino acids were determined for the various periods of the fermentation and presented in Fig. 5.

*Phase I.* Metabolic flux distribution at $t = 6$ h of this period yielded a specific growth rate of 0.015 $h^{-1}$ that is in good agreement with the measured value (Table 1). The specific oxygen uptake rate was determined and showed a 13% error compared with the measured rate. The PP pathway was active and 12% of the glucose was diverted to this pathway. Approximately 61% of biosynthetic redox potential in cytosol was produced by PP pathway. The rest of cytosolic NADPH was produced through the conversion of MnTHF to FTHF (*R*7.3) which was further utilized for nucleotide biosynthesis. The NADPH requirement in the mitochondria for the biosynthesis of isoleucine and other amino acid precursors (i.e., ornithine and α-ketoisovalerate) was completely satisfied by mitochondrial NADP-dependent isocitrate dehydrogenase activity (EC 1.1.1.42). Using ammonia as the nitrogen source, only the NADP-dependent glutamate dehydrogenase enzyme was active leading to glutamate synthesis (*R*6.2). The reported activity of NADP-dependent isoenzyme in *A. oryzae* [15] and *A. nidulans* [51] was much higher than the NAD-dependent isoenzyme.

All amino acids were calculated to have a shadow price of zero (Table 2), indicating that they cannot be used to improve growth during this period. Among the other measured metabolites, however, phosphate was the only nutrient with nonzero and negative shadow price of –1.27 $(\text{mmol/g}_{\text{DW}})^{-1}$. Moreover, all nucleotides (e.g., ATP, CTP) had shadow price of –3.81, indicating a necessity to eliminate surplus energy. In one of the runs, the phosphate uptake rate was allowed to be determined by the optimization algorithm; the free uptake rate was more than four times higher than the measured value. The sensitivity analysis of the result of this run revealed that the shadow price of the nucleotides were still negative but decreased 97% when compared with the original run. This result

**Table 1** Experimental and simulation results of specific growth rate, oxygen uptake rate, and carbon dioxide evolution rate at different phases of cultivation

| | 6 h | | 18 h | | 27 h | | 51 h | |
|---|---|---|---|---|---|---|---|---|
| | Exp. | Sim. | Exp. | Sim. | Exp. | Sim. | Exp. | Sim. |
| $\mu$ ($h^{-1}$) | 0.014 | 0.015 | 0.131 | 0.128 | 0.177 | 0.159 | 0.029 | 0.027 |
| $r_{O_2}(\text{mmol/g}_{\text{DW}}\,h)$ | 8.0 | 6.9 | 8.5 | 6.1 | 4.4 | 3.6 | 0.8 | 0.7 |
| $r_{CO_2}(\text{mmol/g}_{\text{DW}})\,h$ | 0.07 | 0.04 | 0.83 | 0.74 | 1.50 | 1.17 | 0.95 | 0.76 |

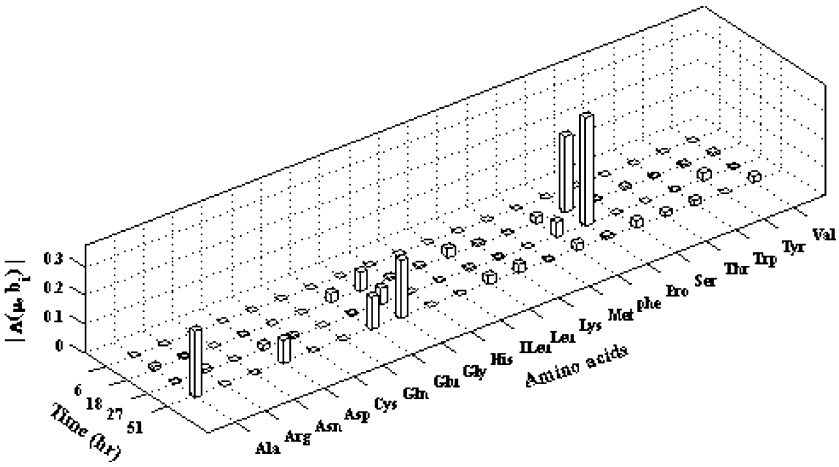


**Fig. 5** Logarithmic sensitivities for amino acids at different phases

indicated that cell growth was limited by phosphate uptake, and not by other measured metabolites including amino acids.

*Phase II*. The flux data corresponding to $t$ = 18 h were used to evaluate the metabolic flux distribution of this phase and it is illustrated in Fig. 6. Since it was not possible to represent all the fluxes, only a summary of the most significant fluxes and those leading to the synthesis of amino acids and organic acids are presented. The optimum specific growth rate was determined to be 0.128 $h^{-1}$ which was 2.3% less than the measured value. Both the specific oxygen uptake rate and carbon dioxide evolution rate were underestimated by 28 and 11% in comparison with the measured values. The carbon flux via PP pathway increased to 19% of the total carbon flux to satisfy the elevated cytosolic NADPH requirements due to the increase in biomass growth rate. The flux through the PP pathway has been reported to increase during high NADPH requirement [52, 53]. Similarly to the first phase, glutamate was produced by NADP-dependent glutamate dehydrogenase enzyme, however, the flux was 2.5 times higher than in Phase I, showing higher requirement of the cells for glutamate. Unlike the first phase, oxaloacetate was generated mainly by the mitochondrial pyruvate carboxylase. A higher production rate of ATP was possible by the higher flux through the reactions of TCA cycle to generate more redox potentials (i.e., NADH and $FADH_2$). The elevated flux through the TCA cycle produced more carbon dioxide, which, in turn, was more likely favoring carbon dioxide fixation inside the mitochondrion.

Cysteine was the only amino acid with shadow price of zero. Since the shadow price of other amino acids were negative, decrease in secretion rate of the by-products (i.e., arginine and serine) or increase in uptake rate of the other amino acids would improve the optimal specific growth rate. In comparison to the previous phase, the shadow price of nucleotides decreased by a factor of 5–10. The shadow price of phosphate was determined to be zero.

Furthermore, an examination of the computed logarithmic sensitivities (Fig. 5) led to some important observations. Although arginine had the highest shadow price amongst the amino acids, its logarithmic sensitivity was very small (< 0.01), so any change in its exchange flux would not significantly affect the optimal growth rate. On the other hand, proline had only a moderate shadow price

**Table 2** Shadow prices for amino acids at different culture phases

| Amino acids | $\lambda_i$ ($g_{DW}$/$mmol_i$) | | | |
|---|---|---|---|---|
| | 6 h | 18 h | 27 h | 51 h |
| Ala | 0.0000 | –0.1393 | –0.1384 | –0.1557 |
| Arg | 0.0000 | –0.5571 | –0.5534 | 0.0000 |
| Asn | 0.0000 | –0.2785 | –0.2767 | –0.3113 |
| Asp | 0.0000 | –0.1393 | –0.1384 | –0.1557 |
| Cys | 0.0000 | 0.0000 | –0.1384 | 0.0000 |
| Gln | 0.0000 | –0.2785 | –0.2767 | –0.3113 |
| Glu | 0.0000 | –0.1393 | –0.1384 | –0.1557 |
| Gly | 0.0000 | –0.1393 | –0.1384 | –0.1557 |
| His | 0.0000 | –0.4178 | –0.4151 | –0.4670 |
| Ileu | 0.0000 | –0.1393 | –0.1384 | –0.1557 |
| Leu | 0.0000 | –0.1393 | –0.1384 | –0.1557 |
| Lys | 0.0000 | –0.2785 | –0.2767 | –0.3113 |
| Met | 0.0000 | –0.1393 | –0.1384 | –0.1557 |
| phe | 0.0000 | –0.1393 | –0.1384 | –0.1557 |
| Pro | 0.0000 | –0.1393 | –0.1384 | –0.1557 |
| Ser | 0.0000 | –0.1393 | –0.1384 | –0.1557 |
| Thr | 0.0000 | –0.1393 | –0.1384 | –0.1557 |
| Trp | 0.0000 | –0.2785 | –0.2767 | –0.3113 |
| Tyr | 0.0000 | –0.1393 | –0.1384 | –0.1557 |
| Val | 0.0000 | –0.1393 | –0.1384 | –0.1557 |

Normal and underlined styles are used for substrates and by-products, respectively

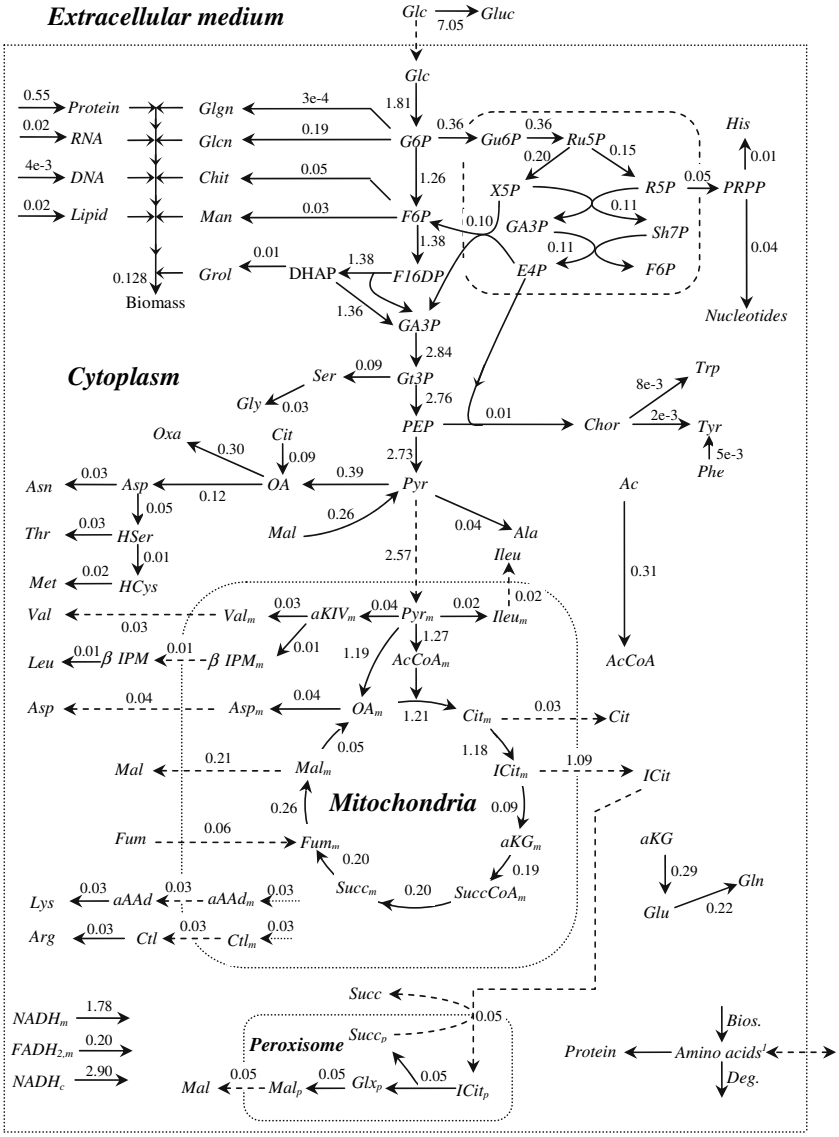


**Fig. 6** Flux distribution map at 18 h (period II). Not all fluxes are shown. Specific flux estimates from measurements taken at 12.0 and 24 h (mmol/$g_{DW}$ h)

but because of its high uptake rate, the optimum value of the objective function was highly sensitive to the proline uptake flux. The highest value of the logarithmic sensitivity among the amino acids was 0.27 for proline. Quantitatively, these values meant that should the uptake rate for this amino acid increases by 10%, then the specific growth rate would increase by 2.7%. Finally, among all measured nutrients, ammonia had the highest logarithmic sensitivity of 0.51, indicating ammonia uptake was growth limiting during this early stage of exponential growth.

*Phase III*. Metabolic flux distribution at the 27th hour of the fermentation was employed as the representative dataset for this phase. The metabolic flux model predicted the specific growth rate reaching a maximum value of 0.159 $h^{-1}$ which showed 10% error relative to the measured value. The fraction of glucose diverted to the PP pathway accounted for 20% of the total uptake rate. The biosynthetic redox potential in the cytosol was mainly supplied by the PP pathway. The mitochondrial pyruvate carboxylase activity was quite significant and accounted for 72% of the total carbon dioxide fixation process. The higher requirement of the cells for ATP caused higher flux through the TCA cycle.

The shadow prices of all amino acids were non-zero and negative. The higher uptake rate of amino acids as energy source (e.g., proline and phenylalanine) and/or lower excretion rate of some (e.g., alanine, aspartate and glycine) would further increase the optimum growth rate. In general, with the exception of ammonia and proline, small logarithmic sensitivities were observed for all measured metabolites. Although, the specific uptake rate of ammonia showed 60% increment relative to the corresponding rate in Phase II it still had the highest logarithmic sensitivity of 0.65 amongst the measured metabolites, and therefore its

uptake was the probable limiting factor for growth. Among the amino acids, proline had the highest logarithmic sensitivity of 0.37.

*Phase IV*. In spite of glucose depletion, the cells continued to grow on gluconate during this phase but at a lower rate than in the previous phase. The predicted specific growth rate by the simulation was determined to be 0.027 $h^{-1}$, which was in excellent agreement with the experimental value of 0.029 $h^{-1}$. The error associated with the predicted specific oxygen uptake was 13%. Both phosphoenolpyruvate carboxinase (EC 4.1.1.32) and glucose-6-phosphatase (EC 3.1.3.9) that would be active during growth on substrates such as ethanol and acetate were also active. The flux of carbon through the PP pathway decreased due to the reduced requirement for biomass formation, however; the PP pathway was responsible for production of 80% of cytosolic NADPH. The activity of the PP pathway was reported to decrease when the need for NADPH production declined [54]. Excepting cysteine and arginine that had zero shadow prices, all amino acids had non-zero negative shadow prices. The highest logarithmic sensitivities were for alanine, glycine, and glutamate which were computed to be 0.23, 0.20, and 0.11, respectively. The relatively high logarithmic sensitivity of glycine was due to its high degradation rate during this period; however, as it was outlined in the "Materials and methods", both the lysozyme and the biomass concentrations were not affected experimentally by changing the glycine concentration even by doubling its concentration for a similar experiment. It could be concluded that glycine catabolism was not coupled directly with biomass formation. Accordingly, glycine was not considered as an important amino acid for further investigations. Interestingly, of all metabolites, ammonia still had the highest logarithmic sensitivity (0.19).

## Discussion

In this study, it was found that tricarboxylic acid cycle was functional throughout the fermentation; however, fluxes were reversed from fumarate to succinate during the lag phase and from oxaloacetate to malate at 27 and 51 h. The mitochondrial pyruvate carboxylase was active throughout the growth phase, whereas the cytosolic carboxylase was active during the first three phases of the fermentation. The glyoxylate shunt was active throughout the fermentation; however, the flux through this shunt was low.

The relative flux through the PP pathway in general depends on the specific growth rate and the medium composition. Our simulation results showed the flux through the PP pathway increased with the specific growth rate from 12 to 20% during the growth phase. In the model simulations, cytosolic NADPH was formed via the PP pathway, through the conversion of MnTHF to FTHF (*R*7.3), as well as the reactions catalyzed by malic enzyme and NADP-dependent isocitrate dehydrogenase. Malic enzyme is known for its regulatory role in the lipid accumulation in filamentous fungi [55] and the reaction catalyzed by this enzyme may be a major source for NADPH synthesis in the cytosol of eukaryotes [41]. However, if the flux through this enzyme was constrained to zero in the model simulations, the flux through the PP pathway increased up to 36%. It is noteworthy that Pedersen et al. [15] reported glucose uptake through the PP pathway to be 38–47% for the recombinant strain and 29–37% for the wild type *A. oryzae* grown in chemostat when they did not consider possible pyruvate formation by malic enzyme. Based on $^{13}C$ trace experiments combined with NMR analysis, the PP pathway flux was estimated to be 53% of the glucose uptake in *A.oryzae* in a chemostat at a specific growth rate of 0.1 $h^{-1}$ [56].

Acetate was the main product of NADP and NAD-dependent acetaldehyde oxidoreductase (EC 1.2.1.5) and its production was concomitant with the production of homocysteine (*R*6.13*d*, EC 2.5.1.49), ornithine (*R*6.25), and oxalic acid (*R*15.3, EC 3.7.1.1) in the network. Since, a significant amount of oxalate was accumulated in the extracellular medium the latter was of great importance for the acetate synthesis. Wild-type *A. niger* was able to catabolize acetate sufficiently fast to prevent its production during oxalate production, while an acetate-non-utilizing mutant was transiently produced some acetate [57]. Our experimental results showed that some acetate was secreted into the extracellular medium by the recombinant strain. In the current model, the rest of the acetate was converted to acetyl-CoA by acetyl-CoA synthase (*R* 10.5*b*). The acetyl-CoA was either entered into the mitochondrion or the peroxisomes compartments. The peroxisomal glyoxylate and acetyl-CoA reacted by the action of malate synthase to form malate (*R*4.7).

The energy requirement for maintenance was stated in the model as the hydrolysis of ATP (*R*.12.1). The results showed that the maintenance requirements accounted for 33% of the total ATP production during the first phase of the fermentation and dropped to essentially zero afterwards. At low growth rates, the microorganisms did not require large amount of energy for metabolic activities and therefore surplus energy was used as maintenance. According to the model, however, the produced ATP was produced for solely metabolic activities.

The concentration profile of glucose and gluconate as the main carbon sources, total amino acids as the organic nitrogen source, and specific growth rate are depicted in Fig. 7. The microorganism showed a diauxic growth pattern which was caused by a shift in metabolic pathways in the middle of the growth cycle. The specific growth rate

increased rapidly during the first 30 h of the fermentation when the glucose served as the main carbon source and the total concentration of amino acids were still high.

After glucose was exhausted, gluconate was the main carbon source. The specific growth rate dropped during this time. Gluconate is an important intermediate of the pentose shunt pathway. Its accumulation was unexpected. One may surmise that the presence of glucose caused the repression of the synthesis of the enzymes that are required for the metabolism of gluconate (e.g. gluconokinase EC 2.7.1.12). During the next 10 h cell mass accumulation was only 2% as the cells adapted to the new carbon source. After this adaptation period, the specific growth rate increased approximately threefold in comparison to its value at 33 h. At this time (i.e., 60 h) the concentration of total amino acids was less than 50% of its initial value, however, the concentration of some amino acids such as alanine, proline, phenylalanine, and cysteine was very low. The concentration of gluconate was still high.

The specific growth rate gradually decreased and reached zero at 78 h as the cells concentration approached its maximum value. One could conclude that the low concentration of the organic nitrogen sources was the main reason for the slow growth immediately after 60 h, while the depletion of both gluconate and amino acids were the reason for the cessation of growth at 78 h. After this time the specific growth rate approached to the small negative values due to cells lysis.

To investigate the importance of experimental flux measurements on model predictions, four sets of flux measurements obtained in four different simulation runs were compared. Table 3 shows the results for the 27th hour of culture. Carbon dioxide evolution rate and oxygen uptake were allowed to be predicted by the model. The experimentally measured fluxes of the specific growth rate, carbon dioxide uptake rate, and oxygen uptake were presented in Table 1.

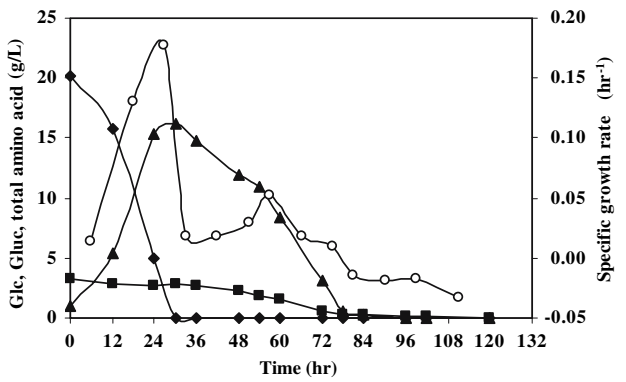


**Fig. 7** Specific growth rate, glucose, gluconate, and total amino acid concentrations as a function of time. Specific growth rate (*open circle*), glucose (*filled diamond*), gluconate (*filled triangle*), and total amino acid (*filled square*)

Run-1 is the typical result of the simulation when the exchange flux of amino acids, organic acids, phosphate, ammonia, and sulfate were implemented in the program as the second set of constraints according to Eq. 3. In Run-2, free uptake rate of amino acids were considered in the simulation. It showed better prediction of the specific growth rate and oxygen uptake rates, whereas the carbon dioxide evolution rate was predicted with less accuracy compared with the first run.

The predicted fluxes of Asn, Gln, His, Leu, Met, and Pro were far from their actual values. Run-3 was performed allowing free uptake rate of amino acids and free excretion rate of organic acids. The same specific growth rate as in Run-2 was observed, while the prediction of carbon dioxide evolution rate was very poor. Besides, the fluxes for Val, His, Pro, OA, Ox, and Gluc were not accurately estimated. The last run, Run-4, was performed without applying any constraint in the optimization program. The calculated fluxes were far from the observed values; however, they represented the maximum capability of the microorganism in biomass production based on the present model. Accordingly, in order to move toward this optimum approach, the exchange fluxes of the organic acids should be reduced to low levels.

Based to the simulation results of Run-4, there was no need for providing the medium with sulfate since the cells were allowed to take up methionine without restriction. Although the last three runs (Run-2, 3, 4) predicted higher specific growth rate than the first one, but the exchange fluxes were not generally in agreement with the real values. Hence, one could conclude that the flux distributions of approaches represented in Run-2, 3, 4 would be unreliable for sensitivity analysis and medium optimization purposes, but could be considered for genetic modification of the strain for higher production of biomass.

Experimental measurements showed that isoleucine, leucine, and phenylalanine uptake rates were higher than the uptake rates of the other amino acids during the first phase of the fermentation. The simulations indicated degradative reactions as the cause of the higher uptake. Also, the sensitivity analysis revealed that their level of uptake rate would not affect the value of the objective function, so the cells might have other applications for the products of the reactions than biomass formation during this phase. Upon further look at the catabolic reactions, it was found that glutamate was the common product of the catabolic reactions for leucine and isoleucine, while tyrosine was the product of phenylalanine. Tyrosine, however, converted to glutamate through another degradation reaction. The high flux through this catabolic reaction was verified by simulation. Furthermore, during the second and third phases,

**Table 3** The value of exchange fluxes between extracellular and intracellular compartments when different set of constraints applied

| Compound | Run-1 | Run-2 | Run-3 | Run-4 |
|---|---|---|---|---|
| $\mu$ | 0.159 | 0.175 | 0.175 | 0.830 |
| $CO_2$ | 1.172 | 0.878 | 0.000 | 11.660 |
| $O_2$ | –3.579 | –4.375 | –3.310 | –15.114 |
| Ala | 0.003 | –0.000 | –0.000 | –0.935 |
| Arg | 0.003 | –0.000 | –0.033 | –0.000 |
| Asn | –0.000 | –1.192 | –0.035 | –0.000 |
| Asp | 0.020 | 0.000 | –0.000 | –0.000 |
| Cyc | 0.009 | –0.008 | –0.000 | –0.039 |
| Gln | –0.000 | –0.154 | –0.000 | –0.000 |
| Glu | 0.007 | –0.000 | –0.000 | –0.338 |
| Gly | 0.065 | –0.000 | –0.000 | –0.000 |
| His | –0.000 | –0.132 | –0.390 | –0.000 |
| Ileu | 0.001 | –0.000 | –0.033 | –3.012 |
| Leu | –0.009 | –1.146 | –0.000 | –0.246 |
| Lys | 0.003 | –0.043 | –0.043 | –0.000 |
| Met | 0.000 | –0.537 | –0.000 | –0.050 |
| Phe | –0.059 | –0.044 | –0.044 | –0.111 |
| Pro | –0.430 | –0.035 | –0.035 | –0.168 |
| Ser | 0.000 | –0.000 | –0.000 | –0.109 |
| Thr | 0.000 | –0.000 | –0.000 | –0.764 |
| Trp | –0.001 | –0.000 | –0.000 | –0.064 |
| Tyr | –0.030 | –0.000 | –0.000 | –0.100 |
| Val | 0.005 | –0.000 | –0.182 | –0.000 |
| Ac | –0.050 | –0.050 | 0.000 | 0.000 |
| a-KG | 0.002 | 0.002 | 0.000 | 0.000 |
| Cit | 0.002 | 0.002 | 0.000 | 0.000 |
| Fum | 0.000 | 0.000 | 0.000 | 0.000 |
| Mal | 0.002 | 0.002 | 0.000 | 0.000 |
| OA | 0.015 | 0.015 | 2.380 | 0.000 |
| Pyr | 0.002 | 0.002 | 0.000 | 0.000 |
| Succ | 0.150 | 0.150 | 0.073 | 0.000 |
| Glun | 0.338 | 0.338 | 0.000 | 0.000 |
| Ox | 0.350 | 0.350 | 0.000 | 0.000 |
| Ammonia | –0.750 | –0.750 | –0.750 | –0.000 |
| Phosphate | –0.126 | –0.126 | –0.126 | –0.654 |
| Sulfate | –0.026 | –0.026 | –0.026 | –0.000 |

All the fluxes are expressed in (mmol/ $g_{D.W.}$ h) except the specific growth rate ($h^{-1}$). The negative and positive numbers show uptake and secretion rates, respectively

proline uptake rate was high due to the high flux through its degradative reaction. Once again, glutamate was the final product of this reaction. In order to investigate which metabolite caused the high demand, one metabolite was eliminated at a time from the proline catabolic pathway in a series of runs with free uptake rate of proline. It was found that when glutamate was eliminated the flux through the degradation reaction was very low. Moreover, the sensitivity analysis revealed that ammonia had the highest logarithmic sensitivity peaking between 12 and 30 h. The high sensitivity of the objective function to ammonia uptake rate could also be due to the demand of the cells for glutamate. Based on the simulation results, the need for high uptake of proline and ammonia could be replaced by an increase of the uptake rate of glutamate alone. Considering all these observations, one could conclude that during the early stages of fermentation glutamate uptake from the extracellular medium was inhibited while the other amino acids and ammonia were more readily transported.

## Validation of model predictions

The predicted and measured biomass concentration profiles are shown in Fig. 8. The biomass concentration was predicted by piecewise integration between two consecutive points. The ability of the proposed model to predict the time profile of the cell density provides verification for the validity of the flux balance model and shows its usefulness for bioprocess design.

The simulation results showed that the higher uptake rate of two amino acids, namely alanine and glutamate benefited biomass production during the last phase, while the higher uptake rate of proline was beneficial during the second and the third phases of the fermentation. Furthermore, the experimental measurements showed that tyrosine was the only amino acid whose concentration decreased approximately to zero after 30 h of the fermentation. When compared to most amino acids, the catabolic flux of tyrosine was determined to be a small value due to its low initial concentration. It could be the reason why it was not recognized as an important amino acid by logarithmic sensitivity analysis. Being a source of glutamate during the degradation process, it was reasonable to investigate the effect of tyrosine on the growth by further experimentation. Four amino acids, namely proline, glutamate, alanine, and tyrosine were recognized as the significant amino acids and could be expected to have the greatest effect on the biomass production rate.

It is worth to note that higher concentrations of the significant metabolites would not necessarily result in higher uptake rate of these metabolites in real situation, because the microorganism may not be capable to take up at higher rates. Since, the sensitivity analysis revealed that the objective function could be increased by flux alteration through certain processes (i.e., bioconversion reactions or exchange reactions) the following experiments were performed as an initial effort to check the capability of the

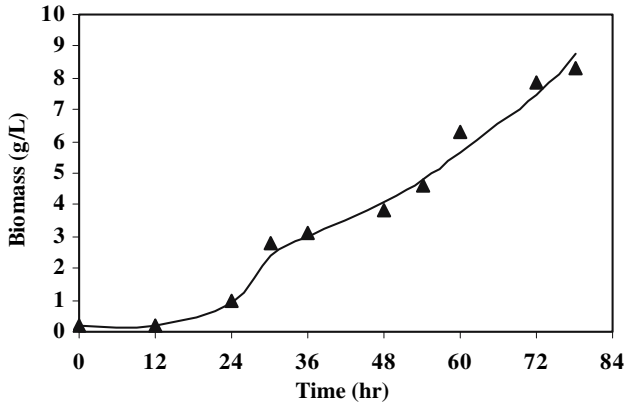


**Fig. 8** The time profile of measured (*filled triangle*) and predicted (*solid line*) biomass concentration. The average relative error between prediction and experimental values was 0.54. $T$ = 27 °C, $N$ = 400 rpm, and aeration 1 vvm

microorganism for higher uptake rate of the aforementioned amino acids. Consequently, a series of growth studies were conducted in shake flasks and the 7 L bioreactor with these amino acids added in excess.

In the preliminary nutritional experiments using shake flasks it was found that the apparent contribution to growth enhancement was 46% for proline, 23% for glutamate, and 22% for tyrosine when these amino acids were added in excess.

Four more experiments were carried out in the 7 L bioreactor with the conditions outlined in "Materials and methods" with the following modifications. The concentration of glucose and the individual amino acids in the first experiment (E-1) was 50% less than those mentioned in the "Materials and methods". The results of this experiment were used as the baseline for comparing results with other medium combinations. The medium composition of the experiments is presented in Table 4.

The extra amount of proline, alanine, and glutamate for E-2, E-3, and E-4 was added to the medium at certain times as determined by the results of the sensitivity analysis. Tyrosine was added at the same time as proline. For instance, any increment in proline uptake rate would enhance the biomass production rate during the second (12–24 h) and the third (24–30 h) phases of the fermentation. Excess proline was added in two steps and 2 h earlier than the start of each period to ensure that no depletion of amino acid occurred.

**Table 4** Medium enrichment with glucose and amino acids

| Experiment | Glucose (g/L) | Proline, alanine, glutamate, tyrosine (g/L) | The rest of amino acids (g/L) |
|---|---|---|---|
| E-1 | 10 | 3 | 4 |
| E-2 | 10 | 8 | 4 |
| E-3 | 20 | 8 | 4 |
| E-4 | 20 | 6 | 8 |

The maximum biomass and lysozyme concentrations observed in each experiment are presented in Fig. 9. Comparison between experiments E-1 and E-2 showed that when the concentration of the significant amino acids increased by a factor of 2.7 while the concentration of the other amino acids and glucose were kept constant the biomass and lysozyme concentrations increased 45 and 41%, respectively. Hence, it seems reasonable to hypothesize that the higher concentration of these amino acids increased their uptake rates, which in turn enhanced the biomass and lysozyme concentrations. These results confirmed the simulation predictions that the specific growth rate was sensitive to any change in the uptake rate of these four amino acids.

The only difference between experiments E-2 and E-3 was the initial glucose concentration, that was 10 and 20 g/L, respectively. In both experiments the concentration of important amino acids were 8 g/L which was the highest level in this series of experiments, while the level of the other amino acids were at the lower level of 4 g/L similar to the basis experiment E-1. It can be seen from the results that the percentage of increment of the biomass concentration increased from 45 to 81% and that of lysozyme concentration from 41 to 82% in comparison to E-2. These observations revealed that when the important organic nitrogen sources were supplied in excess, the higher concentration of glucose had a significant positive effect on both biomass and recombinant protein production.

The initial concentration of the significant amino acids in experiment E-4 was 25% less than in E-2, however, yet it was still high enough to positively affect the production of biomass and recombinant protein. Aside from the

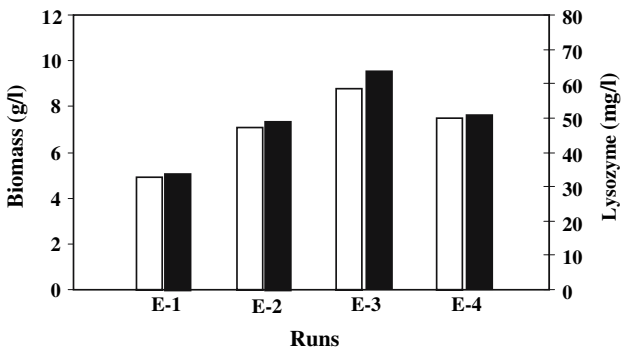


**Fig. 9** The maximum biomass (*open square*) and lysozyme (*filled square*) concentrations observed in the fermentations with the medium compositions presented in Table 4. $T$ = 27 °C, $N$ = 200 rpm, and aeration 1 vvm

concentration of the other amino acids in these two experiments and based on the conclusion in the previous paragraph, one would expect that the biomass and lysozyme concentrations should have been much higher in E-4 than E-2 due to its higher glucose concentration. The experimental results, however, showed that the biomass and lysozyme concentrations in E-4 were only 6 and 4% higher than the corresponding values in E-2. Therefore, one might conclude that the other amino acids not only did not promote the production of biomass and the protein, but most likely had a slightly negative effect on the concentrations.

## Conclusion

A flux-based approach was performed for the analysis of the metabolic network of *A. niger*. A unique aspect of the metabolic network was that it included the participation of carbohydrates and amino acids in both degradative and biosynthetic reactions. The network consisted of 181 biochemical reactions (287 processes) and 137 intracellular metabolites which are distributed among three intracellular compartments. It included glycolysis and pentose phosphate (PP) pathways, tricarboxylic acid cycle (TCA), anaplerotic reactions, ammonia and sulfate assimilation, electron transport reactions, the metabolism of amino acids, biosynthesis of nucleotides, and the biosynthesis of the macromolecular components of biomass such as protein, lipid, RNA, DNA, and carbohydrates.

The proposed model along with the experimental measurements was used to construct the stoichiometric matrix corresponding to the processes with unknown rates. Implementing the model with experimental data as constraints was proven to be necessary for achieving realistic results. Linear programming with experimental constraints was used to determine the optimized specific growth rate at different phases of the fermentation. Flux distribution map for one period of cultivation was presented.

The bioreaction network presented in this study is a general pathway which can be valid for any *A. niger* strain or other aspergilli with some minor modifications. This model can be used not only to find the theoretical metabolic flux distribution, but also to clarify the metabolic behavior of the microorganism along with the experimental data. In this study, the specific growth rate was considered as the optimization objective, but optimization of different objective functions such as ATP, redox potential, and metabolite production can be easily implemented in the model. The model developed in this work was able to predict the specific growth rate very accurately with a maximum error of ±10%. Moreover, oxygen uptake rate and carbon dioxide evolution rate were evaluated with maximum ±28 and ±22% errors, respectively, during the time course of the fermentation. It should be noted that the off-gas analyzer was not able to display the level of oxygen and carbon dioxide in outlet gas accurately, consequently the corresponding experimentally measured fluxes of these two metabolites were less accurate. This could be the reason for the high error percentage associated with these two fluxes. The biomass concentration profile in each period was determined accurately using the corresponding optimal value of the specific growth rate and the standard differential equation which correlates these two parameters.

The performed sensitivity analysis revealed that phosphate uptake was the growth limiting flux during the early stages of the fermentation. Later, the uptake rate of ammonia had a significant effect on the specific growth rate. Among the amino acids proline, alanine, and glutamate had the highest logarithmic sensitivity. In addition, based on the experimental observations tyrosine was a potential candidate to be an effective amino acid. Sensitivity analysis indicated that the other amino acids were not likely to be important for the recombinant protein and biomass production. This was confirmed by experimental observations. The solution of the flux network was very sensitive to ammonia and to a lesser degree to proline during the early stages of exponential phase when glucose was consumed. During this period 10% increase in ammonia and proline uptake rates would increase the specific growth rate by 5–7 and 3–4%, respectively. Alanine, glutamate, and ammonia were limiting nutrients with the highest logarithmic sensitivities among the measured metabolites at the 51st hour of culture. From an operational point of view, one may conclude that the amino acid distribution in peptone was suboptimal with regard to both growth and recombinant protein synthesis. Glucose was found to benefit significantly both biomass and recombinant protein production, especially when the medium contained the important amino acids at their higher levels.

The sensitivity analysis of the specific growth rate with respect to the biomass components revealed that the solution was only sensitive to its protein content. Besides, the analysis showed that the same biomass biosynthesis reaction could be used throughout the fermentation. The results of the metabolic flux analysis may be employed for medium design in continuous or fed-batch operations involving high density culture.

**Acknowledgments** Financial support from the Ministry of Science and Technology of Iran, NSERC, and Cellnet are gratefully acknowledged.

## Appendices

Appendix A: Abbreviations used in metabolic reactions

| | |
|---|---|
| αAAd | α-Aminoadipate |
| Aald | Acetaldehyde |
| Ac | Acetate |
| AclHser | *O*-Acetyl homoserine |
| Acact | Acetoacetate |
| AcCoA | Acetyl coenzyme A |
| ADP | Adenosine 5 diphosphate |
| AICAR | 5-Aminoimidazole-4-carboxamide ribotide |
| αKB | α-Ketobutyrate |
| αKG | α-Ketoglutarate |
| αKIV | α-Ketoisovalerate |
| Ala | L-Alanine |
| Arg | L-Arginine |
| Asn | L-Asparagine |
| Asp | L-Aspartate |
| ATP | Adenosine-5-triphosphate |
| βIPM | β-Isopropylmalate |
| Carp | Carbamoylphosphate |
| Chit | Chitine |
| Chor | Chorismate |
| Cit | Citrate |
| $CO_2$ | Carbon dioxide |
| Ctl | Citruline |
| CTP | Cytidine triphosphate |
| Cys | L-Cysteine |
| DHAP | Dihydroxyacetone phosphate |
| DHF | Dihydrofolate |
| DNA | Deoxyribonucleic acid |
| E4P | Erythrose-4-phosphate |
| EtOH | Ethanol |
| F1,6DP | Fructose-1, 6-diphosphate |
| F6P | Fructose-6-phosphate |
| FAD | Flavine adenine dinucleotide (oxidized) |
| $FADH_2$ | Flavine adenine dinucleotide (reduced) |
| FTHF | Formyltetrahydrofolate |
| Fum | Fumarate |
| GA3P | Glyceraldehyde-3-phosphate |
| G1,3DP | Glycerate-1, 3-diphosphate |
| Glc | Glucose |
| Glgn | Glycogen |
| Gln | L-Glutamine |
| Glu | L-Glutamate |
| Glcn | Glucan |
| Gluc | Gluconic acid |
| Glx | Glyoxylate |
| Gly | L-Glycine |
| Grol | Glycerol |
| G6P | Glucose-6-phosphate |
| GTP | Guanosine triphosphate |
| Gt3P | Glycerate-3-phosphate |
| Gt2p | Glycerate-2-phosphate |
| Gu6P | Gluconate-6-phosphate |
| H | Proton |
| $H_2O$ | Water |
| HCys | Homocysteine |
| His | L-Histidine |
| HSer | Homoserine |
| $H_2S$ | Hydrogen sulfide |
| ICit | Isocitrate |
| Ileu | L-Isoleucine |
| IMP | Inosine monophosphate |
| Leu | L-Leucine |
| Lys | L-Lysine |
| Mal | Malate |
| Man | Mannitol |
| Met | L-Methionine |
| MlTHF | Methyltetrahydrofolate |
| MnTHF | Methylenetetrahydrofolate |
| NAD | Nicotinamide adenine dinucleotide (oxidized) |
| NADH | Nicotinamide adenine dinucleotide (reduced) |
| NADP | Nicotinamide adenine dinucleotide phosphate (oxidized) |
| NADPH | Nicotinamide adenine dinucleotide phosphate (reduced) |
| $NH_3$ | Ammonia |
| $O_2$ | Oxygen |
| Ox | Oxalic acid |
| OA | Oxaloacetate |
| Orn | Ornithine |
| P | Inorganic orthophosphate |
| PEP | Phosphoenolpyruvate |
| Phe | L-Phenylalanine |
| Pro | L-Proline |
| PRPP | 5-Phosphoribosylpyrophosphate |
| Pyr | Pyruvate |
| R5P | Ribose-5-phosphate |
| RNA | Ribonucleic acid |
| Ru5P | Ribulose-5-phosphate |
| SAH | *S*-Adenosylhomocysteine |
| SAM | *S*-Adenosylmethionine |
| Ser | L-Serine |
| SH7P | Sedoheptulose-7-phosphate |
| $SO_4$ | Sulfate |
| Succ | Succinate |
| SuccCoA | Succinyl coenzyme A |
| THF | Tetrahydrofolate |
| Thr | L-Threonine |
| Trp | L-Tryptophane |
| Tyr | L-Tyrosine |
| UDP | Uridine-5-diphosphate |

| | |
|---|---|
| UTP | Uridine triphosphate |
| Val | L-Valine |
| X5P | Xylulose-5-phosphate |

## Appendix B: Metabolic reactions

The letters *b*, *d*, and *g* following the reaction numbers indicate biosynthesis, degradation, and gluconeogenesis reactions. The subscripts *c*, *m*, and *p* show the cytosolic, mitochondrial, and peroxisomal compartments, respectively. $(P/O)^*$ is the stoichiometry of the oxidative phosphorylation of $NADH_c$ and $FADH_{2,m}$ while $(P/O)$ is for $NADH_m$.

*Glycolysis*

$(R1.1)\ Glc_c + ATP_c \Rightarrow G6P_c + ADP_c$

$(R1.1g)\ G6P_c + H_2O_c \Rightarrow Glc_c + P_c$

$(R1.2)\ G6P_c \Leftrightarrow F6P_c$

$(R1.3)\ F6P_c + ATP_c \Rightarrow F1{,}6DP_c + ADP_c$

$(R1.3g)\ F1{,}6DP_c + H_2O_c \Rightarrow F6P_c + P_c$

$(R1.4)\ F1{,}6DP_c \Leftrightarrow DHAP_c + GA3P_c$

$(R1.5)\ DHAP_c \Leftrightarrow GA3P_c$

$(R1.6)\ GA3P_c + NAD_c + P_c \Leftrightarrow G1{,}3DP_c + NADH_c + H_c$

$(R1.7)\ G1{,}3P_c + ADP_c \Leftrightarrow Gt3P_c + ATP_c$

$(R1.8)\ Gt3P_c \Leftrightarrow Gt2P_c$

$(R1.9)\ Gt2P_c \Leftrightarrow PEP_c + H_2O_c$

$(R1.10)\ PEP_c + ADP_c \Rightarrow Pyr_c + ATP_c$

*Pentose phosphate pathway*

$(R2.1)\ G6P_c + NADP_c + H_2O_c \Rightarrow Gu6P_c + NADPH_c + H_c$

$(R2.2)\ Gu6P_c + NADP_c \Rightarrow Ru5P_c + NADPH_c + H_c + CO_{2,c}$

$(R2.3)\ Ru5P_c \Leftrightarrow R5P_c$

$(R2.4)\ Ru5P_c \Leftrightarrow X5P_c$

$(R2.5)\ R5P_c + X5P_c \Leftrightarrow GA3P_c + Sh7P_c$

$(R2.6)\ GA3P_c + Sh7P_c \Leftrightarrow E4P_c + F6P_c$

$(R2.7)\ E4P_c + X5P_c \Leftrightarrow GA3P_c + F6P_c$

*Tricarboxylic cycle pathway*

$(R3.1)\ Pyr_m + ATP_m + CO_{2,m} + H_2O_m \Leftrightarrow OA_m + ADP_m + P_m$

$(R3.2)\ Pyr_m + CoA_m + NAD_m \Rightarrow AcCoA_m + NADH_m + H_m + CO_{2,m}$

$(R3.3)\ AcCoA_m + OA_m + H_2O_m \Rightarrow Cit_m + CoA_m$

$(R3.4)\ Cit_m \Leftrightarrow ICit_m$

$(R3.5)\ ICit_m + NAD_m \Rightarrow \alpha KG_m + NADH_m + H_m + CO_{2,m}$

$(R3.6)\ ICit_c + NAD_c \Rightarrow \alpha KG_c + NADH_c + H_c + CO_{2,c}$

$(R3.7)\ ICit_m + NADP_m \Rightarrow \alpha KG_m + NADPH_m + H_m + CO_{2,m}$

$(R3.8)\ ICit_c + NADP_c \Rightarrow \alpha KG_c + NADPH_c + H_c + CO_{2,c}$

$(R3.9)\ \alpha KG_m + CoA_m + NAD_m \Leftrightarrow SuccCoA_m + NADH_m + H_m + CO_{2,m}$

$(R3.10)\ SuccCoA_m + ADP_m + P_m \Leftrightarrow Succ_m + ATP_m + CoA_m$

$(R3.11)\ Succ_m + FAD_m \Leftrightarrow Fum_m + FADH_{2,m}$

$(R3.12)\ Fum_m + H_2O_m \Leftrightarrow Mal_m$

$(R3.13)\ Mal_m + NAD_m \Leftrightarrow OA_m + NADH_m + H_m$

*Anaplerotic pathways*

$(R4.1)\ Pyr_c + ATP_c + CO_{2,c} + H_2O_c \Leftrightarrow OA_c + ADP_c + P_c$

$(R4.2)\ Cit_c + ATP_c + CoA_c \Rightarrow OA_c + ADP_c + P_c + AcCoA_c$

$(R4.3)\ Mal_c + NADP_c \Rightarrow Pyr_c + CO_{2,c} + NADPH_c + H_c$

$(R4.4)\ Mal_c + NAD_c \Leftrightarrow OA_c + NADH_c + H_c$

$(R4.5)\ PEP_c + ADP_c + CO_{2,c} \Rightarrow OA_c + ATP_c$

$(R4.5g)\ OA_c + ATP_c \Rightarrow PEP_c + ADP_c + CO_{2,c}$

$(R4.6)\ ICit_P \Rightarrow Glx_p + Succ_p$

$(R4.7)\ Glx_p + AcCoA_p + H_2O_c \Rightarrow Mal_p + CoA_p$

*Oxidative Phosphorylation*

$(R5.1)\ NADH_m + H_m + 0.5O_{2,c} + (P/O)ADP_c + (P/O)P_c \Rightarrow NAD_m + (P/O)ATP_c + [(P/O) + 1]H_2O_m$

$(R5.2)\ FADH_{2,m} + 0.5O_{2,m} + (P/O)^*ADP_c + (P/O)^*P_c \Rightarrow FAD_m + (P/O)^*ATP_c + [(P/O)^* + 1]H_2O_m$

$(R5.3)\ NADH_c + H_c + 0.5O_{2,C} + (P/O)^*ADP_c + (P/O)^*P_c \Rightarrow NAD_c + (P/O)^*ATP_c + [(P/O)^* + 1]H_2O_c$

*Amino Acid metabolism*

($R6.1$) $\alpha KG_c + NH_{3,c} + NADH_c + H_c \Leftrightarrow Glu_c + NAD_c + H_2O_c$

($R6.2$) $\alpha KG_c + NH_{3,c} + NADPH_c + H_c \Leftrightarrow Glu_c + NADP_c + H_2O_c$

($R6.3$) $Glu_c + NH_{3,c} + ATP_c \Leftrightarrow Gln_c + ADP_c + P_c$

($R6.4$) $Pyr_c + Glu_c \Leftrightarrow Ala_c + \alpha KG_c$

($R6.5$) $OA_c + Glu_c \Leftrightarrow Asp_c + \alpha KG_c$

($R6.6$) $OA_m + Glu_m \Leftrightarrow Asp_m + \alpha KG_m$

($R6.7$) $Asp_c + Gln_c + 2ATP_c + 2H_2O_c \Leftrightarrow Asn_c + Glu_c + 2ADP_c + P_c$

($R6.8b$) $Glu_c + Gt3P_c + NAD_c + H_2O_c \Rightarrow Ser_c + \alpha KG_c + NADH_c + H_c + P_c$

($R6.8d$) $Ser_c + \alpha KG_c + NADH_c + H_c + ATP_c \Rightarrow Glu_c + Gt3P_c + NAD_c + ADP_c$

($R6.9b1$) $Asp_c + ATP_c + 2NADPH_c + 2H_c \Rightarrow HSer_c + ADP_c + P_c + 2NADP_c$

($R6.9b2$) $Asp_c + ATP_c + NADPH_c + NADH_c + 2H_c \Rightarrow HSer_c + ADP_c + P_c + NADP_c + NAD_c$

($R6.10b$) $HSer_c + ATP_c + H_2O_c \Leftrightarrow Thr_c + ADP_c + P_c$

($R6.10d$) $Thr_c \Rightarrow \alpha KB_c + NH_{3,c}$

($R6.11$) $Ser_c + THF_c \Leftrightarrow Gly_c + MnTHF_c + H_2O_c$

($R6.12$) $SO_{4,c} + 2ATP_c + 4NADPH_c + 4H_c \Rightarrow H_2S_c + 2ADP_c + 2P_c + 4NADP_c + 2H_2O_c$

($R6.13b$) $HSer_c + AcCoA_c \Rightarrow AclHSer_c + CoA_c$

($R6.13d$) $AclHSer_c + H_2S_c \Rightarrow HCys_c + Ac_c$

($R6.14$) $HCys_c + MlTHF_c \Rightarrow Met_c + THF_c$

($R6.15$) $HCys_c + Ser_c \Rightarrow Cys_c + NH_{3,c} + \alpha KB_c$

($R6.16b$) $Ser_c + AcCoA_c + H_2S_c \Rightarrow Cys_c + CoA_c + Ac_c$

($R6.16d$) $Cys_c + AclHSer_c + H_2O_c \Rightarrow HCys_c + NH_{3,c} + Pyr_c$

($R6.17b$) $2Pyr_m + NADPH_m + H_m \Rightarrow \alpha KIV_m + CO_{2,m} + NADP_m + H_2O_m$

($R6.17d$) $\alpha KIV_m + 3NAD_m + CoA_m + 2H_2O_m + FAD_m \Rightarrow 3NADH_m + 3H_m + SuccCoA_m + CO_{2,m} + FADH_{2,m}$

($R6.18$) $\alpha KIV_m + Glu_m \Leftrightarrow Val_m + \alpha KG_m$

($R6.19$) $\alpha KIV_m + AcCoA_m + H_2O_m \Rightarrow \beta IPM_m + CoA_m$

($R6.20b$) $\beta IPM_c + Glu_c + NAD_c \Rightarrow Leu_c + \alpha KG_c + CO_{2,c} + NADH_c + H_c$

($R6.20d$) $Leu_c + \alpha KG_c + ATP_m + CoA_m + NAD_m + FAD_m + 2H_2O_m \Rightarrow Glu_c + ADP_m + P_m + AcCoA_m + NADH_m + H_m + FADH_{2,m} + Acact_m$

($R6.21b$) $Pyr_m + \alpha KB_m + Glu_m + NADPH_m + H_m \Rightarrow ILeu_m + \alpha KG_m + NADP_m + CO_{2,m} + H_2O_m$

($R6.21d$) $ILeu_m + \alpha KG_m + ATP_m + 2CoA_m + 2NAD_m + FAD_m + 2H_2O_m \Rightarrow Glu_m + SuccCoA_m + AcCoA_m + ADP_m + P_m + 2NADH_m + 2H_m + FADH_{2,m}$

($R6.22b$) $Glu_m + AcCoA_m + NAD_m + H_2O_m \Rightarrow \alpha AAd_m + CoA_m + NADH_m + H_m + CO_{2,m}$

($R6.22d$) $\alpha AAd_m + \alpha KG_m + 2CoA_m + 2NAD_m + FAD_m + H_2O_m \Rightarrow Glu_m + 2AcCoA_m + 2NADH_m + 2H_m + FADH_{2,m} + 2CO_{2,m}$

($R6.23b$) $\alpha AAd_c + Glu_c + 2ATP_c + 2NADPH_c + NAD_c + H_c + H_2O_c \Rightarrow Lys_c + \alpha KG_c + 2ADP_c + 2P_c + 2NADP_c + NADH_c$

($R6.23d1$) $Lys_c + \alpha KG_c + NADP_c + H_2O_c \Rightarrow \alpha AAd_c + Glu_c + NADPH_c + H_c$

($R6.23d2$) $Lys_c + \alpha KG_c + NADH_c + 2NADP_c + H_2O_c \Rightarrow \alpha AAd_c + Glu_c + NAD_c + 2NADPH_c + H_c$

($R6.24$) $Gln_c + 2ATP_c + CO_{2,m} + 2H_2O_m \Rightarrow CarP_m + Glu_m + 2ADP_m + P_m$

($R6.25$) $2Glu_m + AcCoA_m + ATP_m + NADPH_m + H_m + H_2O_m \Rightarrow Orn_m + \alpha KG_m + CoA_m + ADP_m + P_m + NADP_m + Ac_m$

($R6.26$) $Carp_m + Orn_m \Leftrightarrow Ctl_m + P_m$

($R6.27b$) $Asp_c + Ctl_c + 2ATP_c + H_2O_c \Rightarrow Arg_c + Fum_c + 2ADP_c + 2P_c$

($R6.27d$) $Arg_c + H_2O_c \Rightarrow Orn_c + CO_{2,c} + 2NH_{3,c}$

($R6.28b$) $Glu_c + ATP_c + 2\,NADPH_c + 2H_c \Rightarrow Pro_c + ADP_c + P_c + H_2O_c + 2NADP_c$

($R6.28d$) $Pro_m + 0.5O_{2,m} + NAD_m + H_2O_m \Rightarrow Glu_m + NADH_m + H_m$

($R6.29$) $R5P_c + 2ATP_c \Leftrightarrow PRPP_c + 2ADP_c$

($R6.30b$) $Gln_c + PRPP_C + ATP_c + 2NAD_c + 5H_2O_c \Rightarrow His_c + \alpha KG_c + AICAR_c + 2NADH_c + 2H_c + 5P_c$

($R6.30d$) $His_c + THF_c + 2H_2O_c \Rightarrow Glu_c + NH_{3,c} + FormiTHF_c$

($R6.31$) $2PEP_c + E4P_c + ATP_c + NADPH_c + H_c \Rightarrow Chor_c + ADP_c + 4P_c + NADP_c$

($R6.32b$) $Gln_c + Ser_c + PRPP_c + Chor_c \Rightarrow Trp_c + Glu_c + GA3P_c + Pyr_c + 2P_c + CO_{2,c} + H_2O_c$

($R6.32d$) $Trp_c + Glu_c + 3O_{2,c} + NADPH_c + H_c + 3H_2O_c \Rightarrow For_c + Ala_c + \alpha KG_c + \alpha AAd_c + CO_{2,c} + NH_{3,c} + NADP_c$

($R6.33b$) $Glu_c + Chor_c + NAD_c \Rightarrow Tyr_c + \alpha KG_c + NADH_c + H_c + CO_{2,c}$

($R6.33d$) $Tyr_c + \alpha KG_c + 2O_{2,c} + H_2O_c$
$\Rightarrow Glu_c + Fum_c + CO_{2,c} + Acact_c$
($R6.34b$) $Glu_c + Chor_c \Rightarrow Phe_c + \alpha KG_c + CO_{2,c} + H_2O_c$
($R6.34d1$) $Phe_c + O_{2,c} + NADPH_c + H_c$
$\Rightarrow Tyr_c + NADP_c + H_2O_c$
($R6.34d2$) $Phe_c + O_{2,c} + NADH_c + H_c$
$\Rightarrow Tyr_c + NAD_c + H_2O_c$
($R6.35$) $\alpha KB_m + ATP_m + H_2O_m + CoA_m + NAD_m$
$\Leftrightarrow SuccCoA_m + ADP_m + P_m + NADH_m + H_m$
($R6.36$) $Thr_c \Leftrightarrow Gly_c + Aald_c$

*Biosynthesis and interconversion of one-carbon units*

($R7.1$) $DHF_c + NADPH_c + H_c \Leftrightarrow THF_c + NADP_c$
($R7.2$) $Gly_c + THF_c + NAD_c$
$\Rightarrow MnTHF_c + NH_{3,c} + CO_{2,c} + NADH_c + H_c$
($R7.3$) $MnTHF_c + NADP_c + H_2O_c$
$\Leftrightarrow FTHF_c + NADPH_c + H_c$
($R7.4$) $MnTHF_c + NADH_c + H_c \Leftrightarrow MlTHF_c + NAD_c$
($R7.5$) $MnTHF_c + NADPH_c + H_c \Leftrightarrow MlTHF_c + NADP_c$
($R7.6$) $Met_c + ATP_c + 2H_2O_c + H_c \Rightarrow SAM_c + 3P_c$
($R7.7$) $SAH_c + 2ATP_c + H_2O_c \Rightarrow HCys_c + 3ADP_c$

*Nucleotides biosynthesis*

($R8.1$) $AICAR_c + FTHF_c \Rightarrow IMP_c + THF_c + H_2O_c$
($R8.2$) $Asp_c + 3ATP_c + IMP_c$
$\Rightarrow ATP^*_c + Fum_c + 3ADP_c + P_c$
($R8.3$) $IMP_c + Gln_c + 4ATP_c + NAD_c + 3H_2O_c$
$\Rightarrow GTP_c + Glu_c + 4ADP_c + NADH_c + H_c + 2P_c$
($R8.4$) $Asp_c + Gln_c + PRPP_c + 4ATP_c + NAD_c + 2H_2O_c$
$\Rightarrow UTP_c + Glu_c + 4ADP_c + NADH_c + H_c + 4P_c$
($R8.5$) $UTP_c + Gln_c + ATP_c + H_2O_c$
$\Rightarrow CTP_c + Glu_c + ADP_c + P_c$
($R8.6$) $PRPP_c + FTHF_c + Gly_c + Asp_c + 2Gln_c + 4ATP_c$
$+ CO_{2,c} + 3H_2O_c \Rightarrow AICAR_c + THF_c + Fum_c$
$+ 2Glu_c + 4ADP_c + 6P_c$
($R8.7$) $UDP_c + ATP_c \Leftrightarrow UTP_c + ADP_c$

*Biomass components*

($R9.1$) $F6P_c + Gln_c + AcCoA_c + UTP_c + H_2O_c$
$\Rightarrow Chit_c + Glu_c + CoA_c + UDP_c + 2P_c$
($R9.2b$) $DHAP_c + NADH_c + H_c + H_2O_c$
$\Rightarrow Grol_c + NAD_c + P_c$
($R9.2d$) $Grol_c + ATP_c + NAD_c$
$\Rightarrow DHAP_c + ADP_c + NADH_c + H_c$
($R9.3b$) $DHAP_c + NADPH_c + H_c + H_2O_c$
$\Rightarrow Grol_c + NADP_c + P_c$
($R9.3d$) $Grol_c + ATP_c + FAD_m$
$\Rightarrow DHAP_c + ADP_c + FADH_{2,m}$
($R9.4b$) $F6P_c + NADH_c + H_c + H_2O_c$
$\Rightarrow Man_c + NAD_c + P_c$
($R9.4d$) $Man_c + ATP_c + NADP_c$
$\Rightarrow F6P_c + ADP_c + NADPH_c + H_c$
($R9.5$) $G6P_c + UTP_c + H_2O_c$
$\Rightarrow Glcn_c + UDP_c + 2P_c$
($R9.6b$) $G6P_c + UTP_c + H_2O_c \Rightarrow Glgn_c + UDP_c + 2P_c$
($R9.6d$) $Glgn_c + P_c \Rightarrow G6P_c$

*$C_2$ compounds metabolism*

($R10.1$) $Aald_c + NADPH_c + H_c \Leftrightarrow EtoH_c + NADP_c$
($R10.2$) $Aald_c + NADH_c + H_c \Leftrightarrow EtoH_c + NAD_c$
($R10.3$) $Aald_c + NADP_c + H_2O_c \Leftrightarrow Ac_c + NADPH_c + H_c$
($R10.4$) $Aald_c + NAD_c + H_2O_c \Leftrightarrow Ac_c + NADH_c + H_c$
($R10.5b$) $Ac_c + CoA_c + 2ATP_c + H_2O_c$
$\Rightarrow AcCoA_c + 2ADP_c + 2P_c$
($R10.5d$) $AcCoA_c + H_2O_c \Rightarrow CoA_c + Ac_c$

*Polymerization reactions*

($R11.1$) $0.095Ala_c + 0.044Arg_c + 0.046Asn_c + 0.046Asp_c$
$+ 0.011Cyc_c + 0.080Gln_c + 0.080Glu_c + 0.094Gly_c$
$+ 0.020His_c + 0.045ILeu_c + 0.069Leu_c + 0.057Lys_c$
$+ 0.014Met_c + 0.031Phe_c + 0.047Pro_c + 0.066Ser_c$
$+ 0.048Thr_c + 0.018Trp_c + 0.028Tyr_c + 0.064Val_c$
$+ 4ATP_c + 4H_2O_c \Rightarrow Protein_c + 4ADP_c + 4P_c$

($R11.2$) $0.256ATP^*_c + 0.196CTP_c + 0.286GTP_c$
$+ 0.262UTP_c + ATP_c + H_2O_c \Rightarrow RNA_c + ADP_c + P_c$

$(R11.3) 0.242ATP_c^* + 0.258CTP_c + 0.258GTP_c + 0.242UTP_c + 1.242NADPH_c + 0.242MnTHF_c + ATP_c + H_2O_c \Rightarrow DNA + 1.242NADP_c + 0.242DHF_c + ADP_c + P_c$

$(R11.4) 18.12AcCoA_c + 0.623DHAP_c + 0.3G6P_c + 1.1SAM_c + 0.4Ser_c + 2.6O_{2,c} + 1.7NADH_c + 22.4NADPH_c + 0.623FADH_{2,m} + 18ATP_c + 18H_2O_c \Rightarrow Lipid_c + 18.12CoA + 1.1SAH_c + 3.8CO_{2,c} + 1.7NAD_c + 22.4NADP_c + 0.623FAD_m + 18ADP_c + 18P_c$

$(R11.5) 4.299Protein_c + 0.194RNA_c + 0.030DNA_c + 0.126Lipid_c + 0.408Chit_c + 1.515Glcn_c + 0.002Glgn_c + 0.213Man_c + 0.090Grol_c + 46.3ATP_c + 46.3H_2O_c \Rightarrow Biomass(1g_{DW}) + 46.3ADP_c + 46.3P_c$

*Maintenance requirements*

$(R12.1)\ ATP_c + H_2O_c \Rightarrow ADP_c + P_c$

*Mitochondrial membrane transport systems*

$(R13.1)\ ATP_m + ADP_c \Leftrightarrow ADP_m + ATP_c$
$(R13.2)\ P_c + H_c \Leftrightarrow P_m + H_m$
$(R13.3)\ Succ_c + Mal_m \Leftrightarrow Succ_m + Mal_c$
$(R13.4)\ ICit_m + Cit_c \Leftrightarrow ICit_c + Cit_m$
$(R13.5)\ Ctl_m + H_c \Leftrightarrow Ctl_c + H_m$
$(R13.6)\ Mal_m + P_c \Leftrightarrow Mal_c + P_m$
$(R13.7)\ ILeu_m + H_c \Leftrightarrow ILeu_c + H_m$
$(R13.8)\ Pyr_c + H_c \Leftrightarrow Pyr_m + H_m$
$(R13.9)\ CO_{2,m} \Leftrightarrow CO_{2,c}$
$(R13.10)\ Fum_c + H_c \Leftrightarrow Fum_m + H_m$
$(R13.11)\ Cit_m + Mal_c \Leftrightarrow Cit_c + Mal_m$
$(R13.12)\ Glu_c + H_c \Leftrightarrow Glu_m + H_m$
$(R13.13)\ Gln_c + H_c \Leftrightarrow Gln_m + H_m$
$(R13.14)\ Val_m + H_c \Leftrightarrow Val_c + H_m$
$(R13.15)\ \beta IPM_m + H_c \Leftrightarrow \beta IPM_c + H_m$
$(R13.16)\ AcCoA_c + CoA_m \Leftrightarrow CoA_c + AcCoA_m$
$(R13.17)\ O_{2,c} \Leftrightarrow O_{2,m}$
$(R13.18)\ Ac_m \Leftrightarrow Ac_c$
$(R13.19)\ \alpha AAd_m \Leftrightarrow \alpha AAd_c$
$(R13.20)\ \alpha KB_c + H_c \Leftrightarrow \alpha KB_m + H_m$
$(R13.21)\ Asp_m + Glu_c \Leftrightarrow Asp_c + Glu_m$
$(R13.22)\ Pro_c + H_m \Leftrightarrow Pro_m + H_c$
$(R13.23)\ Acact_c \Leftrightarrow Acact_m$
$(R13.24)\ Orn_c + H_m \Leftrightarrow Orn_m + H_c$
$(R13.25)\ H_2O_m \Leftrightarrow H_2O_c$

*Peroxisomal membrane transport systems*

$(R14.1)\ Succ_p + ICit_c \Leftrightarrow Succ_c + ICit_p$
$(R14.2)\ ICit_c + Mal_p \Leftrightarrow ICit_p + Mal_c$
$(R14.3)\ Mal_p + H_p \Leftrightarrow Mal_c + H_c$
$(R14.4)\ ATP_c + H_2O_c + H_c \Rightarrow ADP_c + P_c + H_p$
$(R14.5)\ AcCoA_c + CoA_p \Leftrightarrow CoA_p + AcCoA_p$
$(R14.6)\ H_2O_p \Leftrightarrow H_2O_c$

*Other reactions*

$(R15.1)\ Pyr_c \Rightarrow Aald_c + CO_{2,c}$
$(R15.2)\ Clc_c + 0.5O_{2,c} \Rightarrow Gluc_c$
$(R15.3)\ OA_c + H_2O_c \Rightarrow Ox_c + Ac_c$
$(R15.4)\ Gluc_c + ATP_c \Rightarrow Gu6P_c + ADP_c$

## References


1. Archer DB, Jeens DJ, Mackenzie DA, Brightwell G, Lambert N, Lowe G, Radford SE, Dobson CM (1990) Hen egg white lysozyme expressed in, and secreted form, *Aspergillus niger* is correctly processed and folded. Bio/Technology 8:741–745
2. Wiebe MG, Karandikar A, Robson GD, Trinci APJ, Canida JLF, Trappe S, Wallis G, Rinase U, Derkx PKF, Madrid SM, Sinniega H, Faus I, Montijn R, Van den Hondel CAMJJ, Punt PJ (2001) Production of tissue plasminogen activator (t-PA) in *Aspergillus niger* . Biotechnol Bioeng 76:164–174
3. Ward PP, Lo JY, Duke M, May GS, Headon DR, Conneely OM (1992) Production of biologically active recombinant human lactoferrin in *Aspergillus oryzae*. Biotechnology 10:784–789
4. Gyamerah M, Merichetti G, Adedayo O, Scharer JM, Moo-Young M (2002) Bioprocessing strategies for improving hen egg-white lysozyme (HEWL) production by recombinant *Aspergillus niger* HEWL WT-13–16. Appl Microbiol Biotechnol 60:403–407
5. Bartsch S, Schimek C, Wostemeyer J (2002) Microprojectile bombardment as a reliable method for transformation of the mucoralean fungus *Absidia glauca*. Mycoscience 43:213–217
6. Gheshlaghi R, Scharer JM, Moo-Young M, Douglas PL (2005) Medium optimization for hen egg white lysozyme production by recombinant *Aspergillus niger* using statistical methods. Biotechnol Bioeng 90:754–760

7. Li C, Bai J, Cai Z, Ouyang F (2002) Optimization of a cultural medium for bacteriocin production by *Lactococcus lactis* using response surface methodology. J Biotechnol 93:27–34
8. Alvarez-Vasquez F, Gonzalez-Alcon C, Torres NV (2000) Metabolism of citric acid production by *Aspergillus niger*: Model definition, steady-state analysis and constrained optimization of citric acid production rate. Biotechnol Bioeng 70:82–108
9. Vallino JJ, Stephanopoulos GN (1993) Metabolic flux distribution in *Corynebacterium glutamicum* during growth and Lysine overproduction. Biotechnol Bioeng 41:633–646
10. Tacak S, Galik G, Mavituna F, Dervakos G (1998) Metabolic flux distribution for the optimized production of L-glutamate. Enzyme Microb Technol 23:286–300
11. van Gulik WM, de Laat TAM, Vinke JL, Heijnen JJ (2000) Application of metabolic flux analysis for the identification of metabolic bottlenecks in the biosynthesis of Penicillin-G. Biotechnol Bioeng 68:602–618
12. Naeimpoor F, Mavituna F (2000) Metabolic flux analysis in *Streptomyces coelicolor* under various nutrient limitations. Metab Eng 2:140–148
13. KEGG: http://www.kegg.com
14. BRENDA: http://www.brenda.uni-koeln.de/
15. Pedersen H, Carlsen M, Nielsen J (1999) Identification of enzymes and quantification of metabolic fluxes in the wild type and in a recombinant *Aspergillus oryzae* strain. Appl Environ Microbiol 65:11–19
16. Arora DK, Elander RP, Mukerji KG (1992) Handbook of applied mycology, fungal biotechnology (V.4)
17. Martinelli SD, Kinghorn JR (1994) *Aspergillus*: 50 years on. Prog Ind Microbiol 29:61–140
18. Gow NAR and Gadd GM (1995) The growing fungus. Chapman& Hall, UK, pp 211–238
19. Smith JE, Biol FI, Berry DR (1976) The filamentous fungi, vol 2. Biosynthesis and metabolism. Edward Arnold, London
20. David H, Akesson M, Nielsen J (2003) Reconstruction of the central carbon metabolism of *Aspergillus niger*. Eur J Biochem 270:4243–4253
21. Schuurink R, Busink R, Hondmann DH, Witteveen CF, Visser J (1990) Purification and properties of NADP-dependent glycerol dehydrogenase from *Aspergillus nidulans* and *A. niger*. J Gen Microbiol 136:1043–1050
22. Tzagoloff A (1982) Mitochondria. Plenum, New York, pp 199–233
23. Walker JE (1992) The mitochondrial transporter family. Curr Opin Struct Biol 2:519–526
24. Davis RH (1986) Compartmental and regulatory mechanisms in the arginine pathways of *Neurospora crassa* and *Saccharomyces cerecisiae*. Microbiol Rev 50:280–313
25. Lejohn HB (1971) Enzyme regulation, lysine pathways and cell wall structures as indicators of major lines of evolution in fungi. Nature 231:164–168
26. Zabriskie TM and Jackson MD (2000) Lysine biosynthesis and metabolism in fungi. Nat Prod Rep 17: 85–97
27. Zubay G (1988) Biochemistry, 2nd edn. Macmillan, New York
28. Morzycka E and Paszewski A (1982) Cysteine and homocysteine synthesis in *Sacchoromycopsis lipolytica*. Identification and characterization of two cysteine synthases. Acta Biochim Pol 29:81–93
29. Cove DJ (1966) The induction and repression on nitrate reductase in the fungus *Aspergillus nidulans*. Biochem Biophys Acta 113:51–56
30. Archer DB, MacKenzie DA, Ridout MJ (1995) Heterologous protein secretion by *Aspergillus niger* growing in submerged culture as dispersed or aggregated mycelia. Appl Microbiol Biotechnol 44:157–160
31. Mackenzie DA, Gendron LCG, Jeenes DJ, Archer DB (1994) Physiological optimization of secreted protein production by *Aspergillus niger*. Enz Microb Technol 16:276–280
32. Mainwaring DO, Weibe MG, Robson GD, Goldrick M, Jeens DJ, Archer DB, Trinci APJ (1999) Effect of pH on hen egg white lysozyme production and evolution of a recombinant strain of *Aspergillus niger*. J Biotechnol 75:1–10
33. Gawthray GR (2003) An improved reversed-phase liquid chromatographic method for the analysis of low-molecular mass organic acids in plant root exudates. J Chromatogr A 1011:233–240
34. Bidlingmeyer BA, Cohen SA, Tarvin TL (1984) Rapid analysis of amino acids, using precolumn derivatization. J Chromatogr 336:93–104
35. Gheshlaghi R (2007) Optimization of recombinant protein production by a fungal host. PhD thesis, University of Waterloo, Canada.
36. Blumenthal HJ (1968) Glucose catabolism in fungi. Wallerstein Lab Commun 31(106):171–191
37. Lakshminarayana K, Modi VV, Shah VK (1969) Studies of gluconate metabolism in *Aspergillus niger*. Arch Mikrobiol 66:396–405
38. Purohit HJ and Ratledge C (1988) Mitochondrial location of pyruvate carboxylase in *Aspergillus niger*. FEMS Microbiol Lett 55:129–132
39. Bercovitz A, Peleg Y, Battat E, Rokem JS, Goldberg I (1990) Localization of pyruvate carboxylase in organic acid-producing *Aspergillus* strains. Appl Environ Microbiol 56:1594–1597
40. Nielsen J (1997) Physiological engineering aspects of *Penicillium chrysogenum*. World Scientific, Singapore, pp 61–138
41. Stephanopoulos G, Aristidou AA, Nielsen J (1998) Metabolic engineering: principles and methodologies. Academic, San Diego, pp 21–79; 309–351
42. Clarke BL (1980) Stability of complex reaction networks. Adv Chem Phys 43:1–215
43. Dantzig GB, Thapa MN (1997) Linear programming 1: Introduction (Springer series in operations research and financial engineering). Springer, New York
44. Lee SY, Papoutsakis ET (1999) Metabolic engineering. In: Edwards JS, Ramakrishna R, Schilling CH, Palsson BO (eds) Metabolic flux balance analysis. Marcel Dekker, New York, pp 13–58
45. Schilling CH, Letscher D, Palsson BO (2000) Theory for the systemic definition of metabolic pathways and their use in interpreting metabolic function from a pathway-oriented perspective. J Theor Biol 203:229–248
46. Brooke A, Kendrick D, Meeraus A, Raman R (1998) "GAMS: A User's Guide," GAMS Development Corporation, USA
47. Hillier FS, Lieberman GJ (2001) Introduction to operations research, seventh edition. McGraw-Hill, New York, pp 230–284
48. Pannell DJ (1997) Introduction to practical linear programming. Wiley, New York, pp 48–72
49. Torres NV, Voit EO (2002) Pathway analysis and optimization in metabolic engineering. Cambridge University Press, pp 42–73
50. Varma A, Palsson BO (1993) Metabolic capabilities of *Escherichia coli* II. Optimal growth patterns. J Theor Biol 165:503–522
51. Osmani SA, Scrutton C (1983) The sub-cellular localization of pyruvate carboxylase and of some other enzymes in *Aspergillus nidulans*. Eur J Biochem 133:551–560
52. Jorgensen H, Nielsen J, Villadsen J (1995) Metabolic flux distribution in *Peniclillium chrysogenum* during fed-batch cultivations. Biotechnol Bioeng 46:117–131
53. Obanye AIC, Hobbs G, Gardner DCJ, Oliver SG (1996) Correlation between carbon flux through the pentose phosphate pathway and production of the antibiotic methylenomycin in *Streptomyces coelicolor* A3(2). Microbiology 142:133–137
54. dos Santos M, Thygesen G, Kotter P, Olsson L, Nielsen J (2003) Aerobic physiology of redox-engineered *Saccharomyces cerevisiae* strains modified in the ammonium assimilation for increased NADPH availability. FEMS Yeast Res 4:59–68

55. Wynn JP, bin Abdul Hamid A, Ratledge C (1999) The role of malic enzyme in the regulation of lipid accumulation in filamentous fungi. Microbiology 145:1911–1917
56. Schmidt K, Marx A, de Graaf AA, Wiechert W, Sahm H, Nielsen J, Villadesen J (1998) $^{13}$C tracer experiments and metabolite balancing for metabolic flux analysis. Comparing two approaches. Biotechnol Bioeng 58:254–257
57. Ruijter GJG, Van de Vondervoort PJI, Visser J (1999) Oxalic acid production by *Aspergillus niger*: an oxalate-non-producing mutant produces citric acid at pH 5 and in the presence of manganese. Microbiology 145:2569–2576